

# Integrative Learning of Intensity Fluctuations of Quantum Dots under Excitation via a Tailored Mixture Hidden Markov Model

Xin Yang\*   Hawi Nyiera<sup>†</sup>   Yonglei Sun<sup>‡</sup>   Jing Zhao<sup>†</sup>   Kun Chen<sup>\*§</sup>

January 3, 2025

## Abstract

Semiconductor nano-crystals, known as quantum dots (QDs), have garnered significant interest in various scientific fields due to their unique fluorescence properties. One captivating characteristic of QDs is their ability to emit photons under continuous excitation. The intensity of photon emission fluctuates during the excitation, and such a fluctuation pattern can vary across different dots even under the same experimental conditions. What adding to the complication is that the processed intensity series are non-Gaussian and truncated due to necessary thresholding and normalization. As such, conventional approaches in the chemistry literature, typified by single-dot analysis of raw intensity data with Gaussian hidden Markov models (HMM), cannot meet the many analytical challenges and may fail to capture any novel yet rare fluctuation patterns among QDs. Collaborating with scientists in the chemistry field, we have developed an integrative learning approach to simultaneously analyzing intensity series of multiple QDs. Our approach still inherits the HMM as the skeleton to model the intensity fluctuations of each dot, and based on the data structure and the hypothesized collective behaviors of the QDs, our approach asserts that (i) under each hidden state, the normalized intensity follows a 0/1 inflated Beta distribution, (ii) the state distributions are shared across all the QDs, and (iii) the patterns of transitions can vary across QDs. These unique features allow for a precise characterization of the intensity fluctuation patterns and facilitate the clustering of the QDs. With experimental data collected on 128 QDs, our methods reveal several QD clusters characterized by unique transition patterns across three intensity states. The results provide deeper insight into QD behaviors and their design/application potentials.

**Keywords:** Clustering; Integrative learning; Multivariate time series; Zero-one inflation

---

\*Department of Statistics, University of Connecticut, Storrs, CT, USA.

<sup>†</sup>Department of Chemistry, University of Connecticut, Storrs, CT, USA.

<sup>‡</sup>Institute of Materials Science, University of Connecticut, Storrs, CT, USA.

<sup>§</sup>Corresponding author. Email: [kun.chen@uconn.edu](mailto:kun.chen@uconn.edu)

# 1 Introduction

In the fields of chemistry and materials science, semiconductor Nano-crystals, commonly referred to as colloidal quantum dots (QDs), have gained significant attention in recent years. One captivating characteristic of the QDs is their ability to emit photons under photoexcitation, a phenomenon known as fluorescence. The applications of fluorescence property, particularly within the realm of optics and optoelectronics, have spurred extensive research and development efforts. For example, [Li et al. \(2018\)](#) developed a process to construct more efficient quantum LEDs and [Bruns et al. \(2017\)](#) used QDs as photostable probes to track and visualize biological tissues.

The importance of the fluorescence property in applications stems from its abilities to elucidate the intrinsic properties and micro-environment of QDs, particularly at the single QD level. Beyond the aforementioned applications, a more comprehensive understanding of the fluorescence phenomenon would pave the way for designing QDs with specific purposes and providing essential guidelines for the synthesis of novel materials. In turn, this amplifies our focus on rigorous statistical analysis of fluorescence of single QDs, aiming to glean precise insights and optimize its implications.

An intriguing phenomenon of fluorescence of single QDs is “Intensity Intermittency” or “Intensity Fluctuations”, which refers to the observation that the intensity of photon emission fluctuates during excitation, and such fluctuation patterns can vary across different QDs even under the same experimental conditions. Some patterns of intensity fluctuations ([Nirmal et al., 1996](#)) have been observed across various QD types and are well recognized such as Intensity Blinking, in which the intensity shows telegraph-like switching between high and low intensity states. Intensity Flickering has also been reported, in which the intensity exhibits frequent transitions across multiple intensity states. In reality, however, the intensity fluctuation patterns of single QDs are more complex and are not often described with scientific rigor. It is hypothesized that other patterns may exist. Notably, in our data, as depicted in [Figure 1](#), the QDs in the first row are more likely to be of “Flickerin” style,

the QDs in the second row exhibit more behaviors of “Blinking”, while the QDs in the last row show characteristics of neither fluctuation types.

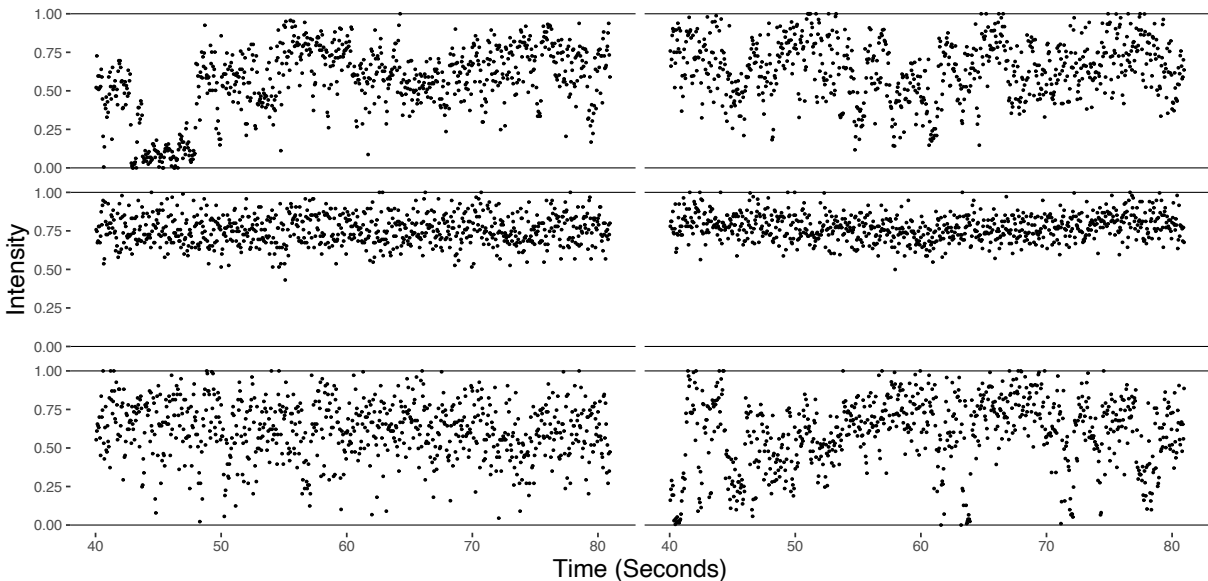


Figure 1: Intensity fluctuation patterns in quantum dots.

In chemistry literature, researchers often conduct single-dot analysis of raw intensity series data, with, e.g., Gaussian hidden Markov models (HMM) (McKinney et al., 2006a). As the overall intensity level varies across QDs, the resulting high, medium, and low intensity states from HMMs could also vary across QDs. Their selection, labeling, and correspondence can then be arbitrary and often rely on the experiences of the researcher. In more recent studies, some advanced analytical methods have been developed, encompassing probability distribution analysis (Efros and Rosen, 1997; Kuno et al., 2000), burst variance analysis (Frantsuzov et al., 2008), FRET two-kernel density estimator (Sisamakris et al., 2010), and fluorescence correlation spectroscopy (Magde et al., 1972; Mücksch et al., 2018). While each of these methods focuses on elucidating the fluctuation patterns of individual QDs, they tend to overlook the aspect of similarity across different QDs. As such, they can’t meet the many analytical challenges and may fail to capture any novel yet rare fluctuation patterns among QDs. Collaborating with scientists in chemistry, we innovate an integrative learning pipeline

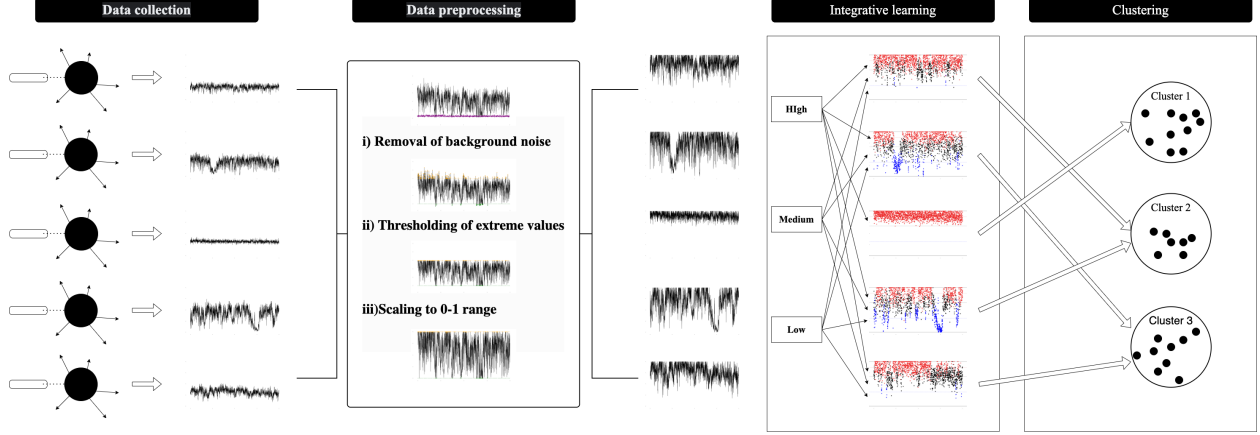


Figure 2: Proposed pipeline of quantum dot analysis from data collection, data processing, to integrative analysis with MHMM.

(as shown in Figure 2) to simultaneously analyze standardized and robustified intensity series of multiple QDs. To achieve this, we first develop a data pre-processing procedure based on the scientific experiment, by eliminating background noise from the intensity values and thresholding and normalizing raw intensity values to remove the inherent variation between different QDs. After rescaling, the intensity values in each series then become bounded between 0 and 1 and can be exactly either 0 or 1. At the end of the pipeline, the processed intensities are analyzed integratively using our proposed approach, where the state identification and clustering are performed iteratively.

Our analytic approach still inherits the HMM as the skeleton, that is, for each dot, we assume the intensity fluctuations are governed by a set of unobserved hidden states that operate as a Markov chain. We further assume that (1) under each state, the standardized intensity follows a 0/1 inflated Beta distribution based on empirical evidence, (2) the hidden state distributions are shared across all the QDs to enable integrative learning, and (3) the patterns of transitions can vary across QDs thus giving rise to a mixture HMM (MHMM). These features lead to a precise characterization of the intensity fluctuation patterns and facilitate an objective clustering of the QDs.

The remainder of the paper is organized as follows. In Section 2, we describe the data and

the problem setup for studying the intensity fluctuations. In Section 3, after an overview of existing methods, we propose the MHMM model with inflated Beta distribution and briefly discuss its computation and theoretical properties. Extensive simulation studies are presented in Section 4. In Section 5, we thoroughly discuss the results of analyzing our QD dataset. In Section 6, we provide a few concluding remarks and discuss future works.

## 2 Data and Pre-Processing Pipeline

The data were compiled from 128 quantum dot samples. For each QD, we obtained 2000 intensity measurements across a 100-second time frame. In the following, we detail the data acquisition and processing methodology.

### 2.1 Data Acquisition

The QD samples, specifically CsPbBr<sub>3</sub> Perovskite Nanocrystals, were synthesized following the method from [Protesescu et al. \(2015\)](#). These samples were then diluted in a 3% w/v polystyrene in toluene solution, deposited onto coverslips through spin casting, and examined under a Nikon Eclipse Ti-u microscope. Excitation of QDs was achieved using a 405 nm pulsed diode laser, with the resulting photo-luminescence filtered through a 510±40 nm band-pass filter. A time-correlated single photon counting module recorded the photo-luminescence in time-tagged time-resolved (TTTR) mode, capturing photon arrival time. Intensity was then calculated as the number of photons detected over a given time period divided by the length of that period.

### 2.2 Pre-Processing

The raw intensity data that we obtained present several aspects of heterogeneity and irregularity, including the varying magnitudes of the intensity values between the QDs and the presence of outlying values. We closely collaborated with chemists to design a data

standardization procedure as follows.

1. Removal of background noise: For each QD, the average intensity of the background is estimated and subtracted from the raw intensity values.
2. Thresholding of extreme values: For each QD, the intensity threshold is set as the average of its 90th percentile and its maximum background-free intensity. Intensity values below zero are reset to zero, while those above the threshold were capped at the threshold value.
3. Scaling: For each QD, the intensity values are scaled to the 0-1 range by dividing its maximum value.

We stress that the data preprocessing procedure described above is based on the nature of the chemical experiments and is deemed justifiable by our close collaborators in chemistry. This procedure yields a standardized dataset where each intensity series consists of 2000 equally-spaced intensity values for a 100-second time frame and with all the values ranging from 0 to 1 (inclusive). This makes a direct comparison across the QDs possible.

Table 1 presents some summary statistics for standardized intensity measurements. It indicates that the mean intensity values of the QDs are relatively concentrated, with a median of 0.694 and an interquartile range of 0.614 to 0.774. Additionally, the zero rate and the one rate remain low, with a maximum of 0.021, suggesting very limited occurrences of extreme values in the intensity values. These confirm that the standardized intensity values are comparable across the QDs. Furthermore, recall that Figure 1 shows that QDs may exhibit distinctive behaviors of intensity fluctuation over time. We therefore aim to perform an integrative learning of all QDs to reveal the unique yet interrelated intensity fluctuation mechanisms and potential clusters of the QDs.

Table 1: Summary statistics of standardized intensity series.

	Min	25 <sup>th</sup> Percentile	Median	75 <sup>th</sup> Percentile	Max
Mean Intensity	0.480	0.614	0.694	0.774	0.833
Zero Rate	0.000	0.000	0.000	0.000	0.038
One Rate	0.002	0.009	0.011	0.014	0.021

### 3 Integrative Learning of Intensity Fluctuations of QDs

#### 3.1 Overview

In the chemistry literature, researchers often analyze the dynamics and intensity fluctuations of each single QD. For example, [McKinney et al. \(2006b\)](#) introduced an HMM approach, assuming that different trajectories shared a homogeneous transition pattern. Consequently, their approach involved fitting an HMM model to each (representative) trajectory and calculating the average transition matrices. [Pirchi et al. \(2016\)](#) utilized an H<sup>2</sup>MM framework, an enhanced version of HMM. The novelty of their approach lied in the consideration of hidden state transitions and non-transition times; two sets of hidden states were assigned – one for transitions and another for non-transitions. These HMM based single-dot approaches allow for the classification of intensity levels into discrete states, such as high, medium, and low. However, challenges arise because intensity levels vary across QDs, leading to subjective labeling and reliance on researcher expertise for state correspondence. While HMMs provide valuable insights into individual QDs, they lack the capacity to analyze patterns across multiple QDs simultaneously, missing opportunities to identify shared behaviors or rare but novel anomalies.

To address data heterogeneity, finite mixture models ([Dempster et al., 1977](#)) have been widely adopted in various fields, including medicine ([Schlattmann and Böhning, 1993](#)), public health ([Fahey et al., 2011](#)), psychology ([Steinley and Brusco, 2011](#)), and economics ([Deb et al., 2011](#); [Deb and Trivedi, 1997](#)). These models decompose data into a weighted sum of distributions, each representing a cluster, thereby capturing group-level patterns. The integration of HMMs and mixture models, particularly in the form of Mixture Hidden Markov

Models (MHMMs), has shown promise in addressing temporal and cluster-level complexities. MHMMs extend HMMs by allowing the transition dynamics to vary across clusters, enabling simultaneous state identification and clustering. Historically, MHMMs have been mainly applied to Gaussian data, such as in neuroscience to classify EEG signals (Wang et al., 2018) or in economics to study market volatility (Dias et al., 2010). However, Gaussian assumptions are often unsuitable for datasets like QD intensities, where distributions exhibit bounded behavior and inflation at extreme values (e.g., 0 and 1).

### 3.2 Mixture HMM with Inflated Beta

We consider a set of  $N$  QD samples, where each QD is associated with intensity values at  $T$  different time points. Let  $x_{i,t}$  denote the intensity of  $i^{\text{th}}$  QD at time  $t$ , where  $i \in \{1, \dots, N\}$  and  $t \in \{1, \dots, T\}$ . Correspondingly, the vector  $\mathbf{x}_i = (x_{i,1}, \dots, x_{i,T})^{\text{T}}$  denotes the intensity series of dot  $i$  and the matrix  $\mathbf{X} = (\mathbf{x}_1, \dots, \mathbf{x}_N)^{\text{T}}$  consists of all the observed QD intensity series.

Our approach inherits the HMM as the skeleton, that is, for each dot, we assume the intensity fluctuations are governed by a set of unobserved hidden states that operate as a Markov chain. With  $M$  states, the state of the intensity  $x_{i,t}$  can be represented as a vector  $\mathbf{s}_{i,t} = (s_{i,t,1}, \dots, s_{i,t,M})^{\text{T}}$ , where  $s_{i,t,h}$ ,  $h = 1, \dots, M$ , are indicator variables and  $s_{i,t,h} = 1$  only if  $x_{i,t}$  is at state  $h$ . We use  $\mathbf{s}_i = (\mathbf{s}_{i,1}, \dots, \mathbf{s}_{i,T})^{\text{T}}$  to represent the state series of  $\mathbf{x}_i$  and use  $\mathbf{S} = (\mathbf{s}_1, \dots, \mathbf{s}_N)^{\text{T}}$  to collect state series for all the intensity series.

With the above general HMM setup, we impose several tailored structures for the integrative analysis of the QDs. First, we assume that under each state, the standardized intensity follows a 0/1 inflated Beta distribution. That is, the probability density function of the intensity under state  $h$  is written as

$$\begin{aligned} & f(x_{i,t} \mid s_{i,t,h} = 1, a_{i,h}, b_{i,h}, \epsilon_{i,h}^{(0)}, \epsilon_{i,h}^{(1)}) \\ &= (\epsilon_{i,h}^{(0)})^{I(x_{i,t}=0)} [(1 - \epsilon_{i,h}^{(0)} - \epsilon_{i,h}^{(1)}) f(x_{i,t} \mid a_{i,h}, b_{i,h})]^{I(0 < x_{i,t} < 1)} (\epsilon_{i,h}^{(1)})^{I(x_{i,t}=1)}, \end{aligned}$$



where  $\epsilon_{i,h}^{(0)} = P(x_{i,t} = 0 \mid s_{i,t,h} = 1)$  and  $\epsilon_{i,h}^{(1)} = P(x_{i,t} = 1 \mid s_{i,t,h} = 1)$  are the inflated probabilities, and  $f(x_{i,t} \mid a_{i,h}, b_{i,h})$  is the density function of the Beta distribution,  $\text{Beta}(a_{i,h}, b_{i,h})$ .

Based on the chemical process, it is expected that each QD only has a few intensity states, in particular, three states representing relatively low, median, and high intensities. Since all data are standardized, we further assume that the possible intensity states are shared across all the QDs, that is, the parameters of the inflated Beta distributions no longer depend on  $i$ , so that the probability density function under state  $h$ ,  $h = 1, \dots, M$ , can be simplified as

$$\begin{aligned} & f(x_{i,t} \mid s_{i,t,h} = 1, a_h, b_h, \epsilon_h^{(0)}, \epsilon_h^{(1)}) \\ &= (\epsilon_h^{(0)})^{I(x_{i,t}=0)} [(1 - \epsilon_h^{(0)} - \epsilon_h^{(1)}) f(x_{i,t} \mid a_h, b_h)]^{I(0 < x_{i,t} < 1)} (\epsilon_h^{(1)})^{I(x_{i,t}=1)}, \end{aligned} \quad (1)$$

This effectively enables integrative learning, as now the potential intensity states are to be collectively identified from all the QDs.

It is now in order to capture the heterogeneity in the intensity fluctuation across the QDs. We achieve this by considering the transition patterns in the hidden Markov process and assuming that the state transition probabilities can vary across QDs. This gives rise to a mixture HMM (MHMM), with which all QDs can be clustered into  $K$  clusters/groups, each characterized by a unique state transition or fluctuation pattern. Specifically, let the cluster number of each dot  $i$  be represented by a vector  $\mathbf{z}_i = (z_{i,1}, \dots, z_{i,K})^T$ , where  $z_{i,k} = 1$  if dot  $i$  belongs to group  $k$  and otherwise  $z_{i,k} = 0$ , for  $k = 1, \dots, K$ ,  $i \in \{1, \dots, N\}$ , and let  $\mathbf{Z} = (\mathbf{z}_1, \dots, \mathbf{z}_N)^T$ . Let  $\delta_k = Pr(z_{i,k} = 1)$ ,  $k = 1, \dots, K$ , with  $\sum_{k=1}^K \delta_k = 1$ . For each cluster, we use  $\mathbf{\Pi}_k$  to denote the transition matrix, where its element  $(\mathbf{\Pi}_k)_{p,q}$  gives the probability of switching to state  $q$  from state  $p$ , i.e.,  $(\mathbf{\Pi}_k)_{p,q} = Pr(s_{i,t,q} = 1 \mid s_{i,t-1,p} = 1)$ . We also use  $\mathbf{\Pi}$  to denote the collection of all the transition matrices  $\mathbf{\Pi}_k$ ,  $k \in \{1, \dots, K\}$ .

We term the proposed method as the *integrative mixture hidden Markov model with 0/1 inflated Beta*, denoted as MHMM- $\beta$ . The tailored model structures imposed above lead to a precise characterization of the intensity fluctuation patterns and facilitate an objective clustering of the QDs. To summarize and visualize, Figure 3 shows a conceptual diagram of

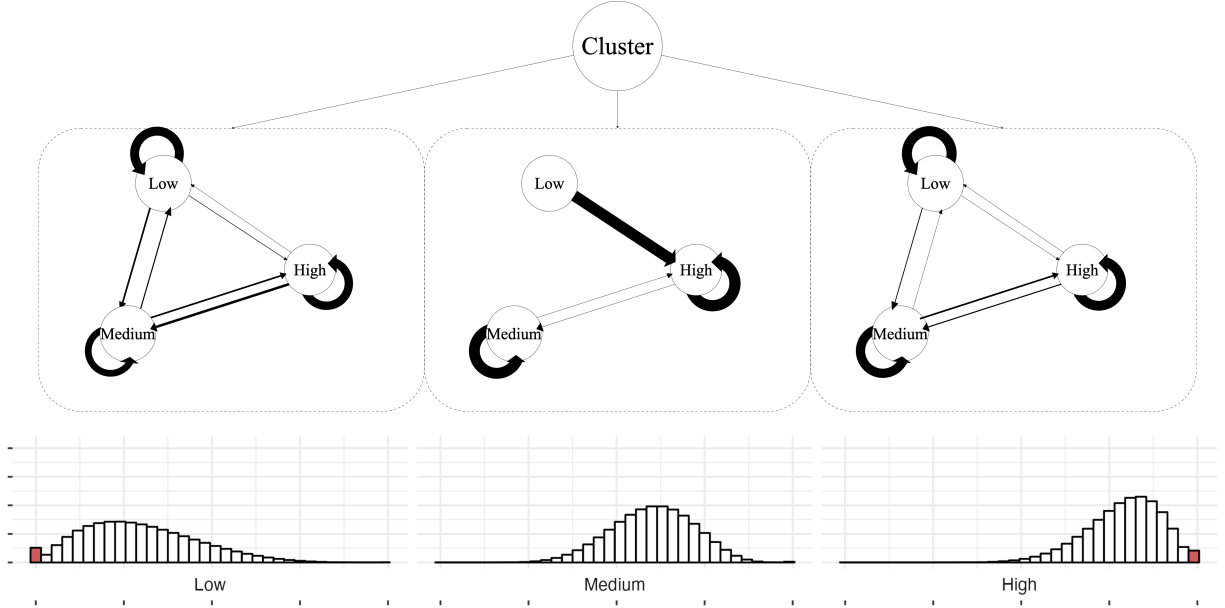


Figure 3: Schematic illustration of the integrative mixture hidden Markov model with 0/1 inflated Beta (MHMM- $\beta$ ).

the proposed MHMM- $\beta$  model. The clusters share the same set of three hidden states and are distinguished by three different transition patterns. The three shared states, i.e., the three inflated Beta distributions, are shown by the three histograms at the bottom of the figure. The potential transitions are represented by the arrows with the thickness indicating the magnitude of the probability. A QD in Cluster 1 tends to stay in its current state and rarely transits to other states, while a QD in Cluster 2 may always transit to the high state from the low state (essentially it means that the QD does not spend any time in the low state).

### 3.3 Likelihood Derivation and Estimation Criterion

Here we derive the likelihood function and discuss maximum likelihood estimation with the EM algorithm.

To proceed, we use  $\pi_{k,s_{i,1}}$  to denote the probability of the initial state when the  $i$ th QD is in the  $k$ th cluster, such that  $\pi_{k,h} = Pr(s_{i,1,h} = 1 \mid z_{i,k} = 1)$  and  $\sum_{h=1}^M \pi_{k,h} = 1$ . Let

$\boldsymbol{\pi}_k = (\pi_{k,1}, \dots, \pi_{k,M})^\top$ , and  $\boldsymbol{\pi} = (\boldsymbol{\pi}_1, \dots, \boldsymbol{\pi}_K)^\top$ . Let  $\Theta$  denote the set of all the unknown parameters, including the parameters for the state distributions  $(\epsilon_h^{(0)}, \epsilon_h^{(1)}, a_h, b_h)_{h=1, \dots, M}$ , the parameters in the transition matrices  $(\mathbf{\Pi}_k)_{k=1, \dots, K}$ , and the parameters for the initial states  $\boldsymbol{\pi}$ .

Two key properties of the Markov chain are utilized. First, the sequence  $(s_{i,1}, \dots, s_{i,T})$  forms a Markov chain if  $s_{i,t+1} \perp (s_{i,1}, \dots, s_{i,t-1}) \mid s_{i,t}$ , meaning that the future is conditionally independent of the past given the present state. Second, the condition  $x_{i,t} \perp (s_{i,1}, \dots, s_{i,t-1}, x_{i,1}, \dots, x_{i,t-1}) \mid s_{i,t}$  holds, meaning that the present observation depends only on the present state. With these properties and the inflated Beta distribution defined in (1), the complete-data likelihood of each dot  $i$ , given the intensity series  $\mathbf{x}_i$ , the state series  $\mathbf{s}_i$ , and the cluster information  $\mathbf{z}_i$ , is given by

$$L(\Theta \mid \mathbf{x}_i, \mathbf{s}_i, \mathbf{z}_i) = \prod_{k=1}^K \left\{ \delta_k \pi_{k, \mathbf{s}_{i,1}} f(x_{i,1} \mid \mathbf{s}_{i,1}) \prod_{t=2}^T (\mathbf{\Pi}_k)_{\mathbf{s}_{i,t-1}, \mathbf{s}_{i,t}} f(x_{i,t} \mid \mathbf{s}_{i,t}) \right\}^{I(z_{i,k}=1)}, \quad (2)$$

where  $f(x_{i,t} \mid \mathbf{s}_{i,t})$  is the density function of the state, i.e.,  $f(x_{i,t} \mid s_{i,t,h} = 1) = f(x_{i,t} \mid s_{i,t,h} = 1, a_h, b_h, \epsilon_h^{(0)}, \epsilon_h^{(1)})$  as defined in (1). Then the complete-data likelihood function for all dots can be written as  $L(\Theta \mid \mathbf{X}, \mathbf{S}, \mathbf{Z}) = \prod_{i=1}^N L(\Theta \mid \mathbf{x}_i, \mathbf{s}_i, \mathbf{z}_i)$ .

Both  $\mathbf{s}_i$  and  $\mathbf{z}_i$  are unobserved. From the complete-data likelihood function (2), the unobserved parts can be integrated out, leading to the observed data likelihood,

$$L(\Theta \mid \mathbf{x}_i) = \sum_{k=1}^K \left[ \delta_k \sum_{\mathbf{s}_i \in \mathcal{S}_i} \left\{ \pi_{k, \mathbf{s}_{i,1}} f(x_{i,1} \mid \mathbf{s}_{i,1}) \prod_{t=2}^T (\mathbf{\Pi}_k)_{\mathbf{s}_{i,t-1}, \mathbf{s}_{i,t}} f(x_{i,t} \mid \mathbf{s}_{i,t}) \right\} \right], \quad (3)$$

where  $\mathcal{S}_i$  stands for all the possible state sequences for dot  $i$ . As a key part to calculate the observed data log-likelihood, the summation of all possible sequences of hidden states is calculated using the forward probabilities (Rabiner, 1989). More details can be found in Section 3.4.

The likelihood function for all dots with the observed data is given by  $L(\Theta \mid \mathbf{X}) =$

$\prod_{i=1}^N L(\Theta | \mathbf{x}_i)$ . We then propose to conduct the maximum likelihood estimation:

$$\hat{\Theta} = \arg \max_{\Theta} \log(L(\Theta | \mathbf{X})) = \arg \max_{\Theta} l(\Theta | \mathbf{X}). \quad (4)$$

where  $l(\Theta | \mathbf{X}) = \sum_{i=1}^N \log L(\Theta | \mathbf{x}_i)$  is the log-likelihood function.

## 3.4 Computational Algorithm & Model Selection

### 3.4.1 Computational Algorithms

We derive an EM algorithm for optimization, which executes an E-step and an M-step iteratively until convergence.

The procedures of the E-Step are shown as follows. First, we utilize the complete-data log-likelihood function in (2) and the multiple expectation structure to define the conditional expectation function of the complete-data log-likelihood (5),

$$\begin{aligned} Q(\Theta | \Theta^{(j)}) &= E_{(\mathbf{S}, \mathbf{Z}) \sim p(\cdot, \cdot | \mathbf{X}, \Theta^{(j)})} [l(\Theta | \mathbf{X}, \mathbf{S}, \mathbf{Z}) | \mathbf{X}, \Theta^{(j)}] \\ &= E_{\mathbf{S} \sim p(\cdot | \mathbf{X}, \mathbf{Z}, \Theta^{(j)})} \{ E_{\mathbf{Z} \sim p(\cdot | \mathbf{X}, \Theta^{(j)})} [l(\Theta | \mathbf{X}, \mathbf{S}, \mathbf{Z})] \}, \end{aligned} \quad (5)$$

where  $\Theta^{(j)}$  stands for the estimated parameters from  $j$ th iteration. In (5), the multiple integration part is simplified into a double expectation structure. As a prerequisite for the E-step, we adopt the idea of dynamic programming (Rabiner, 1989) to define forward-backward probabilities,

$$\begin{aligned} \alpha_{i,t,k,h} &= Pr[(x_{i,1}, \dots, x_{i,t})^T, s_{i,t,h} = 1 | z_{i,k} = 1, \Theta^{(j)}], \\ \beta_{i,t,k,h} &= Pr[(x_{i,t+1}, \dots, x_{i,T})^T, s_{i,t,h} = 1 | z_{i,k} = 1, \Theta^{(j)}]. \end{aligned}$$

Borrowing the notations from Rabiner (1989), the quantities that need to be computed in

the E-step is listed below:

$$\begin{aligned}
\tau_{i,k}(\Theta^{(j)}) &= E[I(z_{i,k} = 1) \mid \mathbf{x}_i, \Theta^{(j)}], \\
\xi_{i,t,k,p,q}(\Theta^{(j)}) &= E[I(s_{i,t-1,p} = 1, s_{i,t,q} = 1 \mid z_{i,k} = 1, \mathbf{x}_i, \Theta^{(j)})], \\
\gamma_{i,t,k,h}(\Theta^{(j)}) &= E[I(s_{i,t,h} = 1) \mid z_{i,k} = 1, \mathbf{x}_i, \Theta^{(j)}], \\
\eta_{i,t,h}(\Theta^{(j)}) &= E[I(s_{i,t,h} = 1) \mid \mathbf{x}_i, \Theta^{(j)}].
\end{aligned}$$

Consequently, we have that

$$\begin{aligned}
Q(\Theta \mid \Theta^{(j)}) &= \sum_{i=1}^N \sum_{k=1}^K \tau_{i,k}(\Theta^{(j)}) \log(\pi_{k,s_{i,1}}) \\
&+ \sum_{i=1}^N \sum_{k=1}^K \tau_{i,k}(\Theta^{(j)}) \left\{ \sum_{t=2}^T \sum_{p=1}^M \sum_{q=1}^M \xi_{i,t,k,p,q}(\Theta^{(j)}) \log(\Pi_k)_{p,q} \right\} \\
&+ \sum_{i=1}^N \sum_{k=1}^K \tau_{i,k}(\Theta^{(j)}) \left\{ \sum_{t=1}^T \sum_{p=1}^M \gamma_{i,t,k,p}(\Theta^{(j)}) \log f(x_{i,t} \mid s_{i,t,p} = 1) \right\}.
\end{aligned}$$

The M-step then maximizes  $Q(\Theta \mid \Theta^{(j)})$  to update the parameters, which leads to

$$\begin{aligned}
\delta_k^{(j+1)} &= \frac{\sum_{i=1}^N \tau_{i,k}(\Theta^{(j)})}{N}, \\
(\Pi_k)_{p,q}^{(j+1)} &= \frac{\sum_{i=1}^N \tau_{i,k}(\Theta^{(j)}) \left\{ \sum_{t=2}^T \xi_{i,t,k,p,q}(\Theta^{(j)}) \right\}}{\sum_{i=1}^N \tau_{i,k}(\Theta^{(j)}) \left\{ \sum_{t=2}^T \sum_{q'=1}^M \xi_{i,t,k,p,q'}(\Theta^{(j)}) \right\}}, \\
(\epsilon_h^{(r)})^{(j+1)} &= \frac{\sum_{i=1}^N \sum_{k=1}^K \tau_{i,k}(\Theta^{(j)}) \sum_{t=1}^T \gamma_{i,t,k,h}(\Theta^{(j)}) I(x_{i,t} = r)}{\sum_{i=1}^N \sum_{k=1}^K \tau_{i,k}(\Theta^{(j)}) \sum_{t=1}^T \gamma_{i,t,k,h}(\Theta^{(j)})} \quad \text{for } r \in \{0, 1\}, \\
(a_h^{(j+1)}, b_h^{(j+1)}) &= \arg \max_{(a_h, b_h)} \sum_{i=1}^N \sum_{k=1}^K \tau_{i,k}(\Theta^{(j)}) \left\{ \sum_{t=1}^T \gamma_{i,t,k,h}(\Theta^{(j)}) \right\}.
\end{aligned} \tag{6}$$

The last problem in (6) can be solved by a Newton-Raphson algorithm.

All the details of the proposed EM algorithm are given in Section A of the Supplementary Material.

### 3.5 Model Selection & Inference

For selecting the number of clusters and the number of states, several information criteria are available, including AIC (Akaike, 1974), BIC (Schwarz, 1978), and the Integrated Completed Likelihood (ICL) (Biernacki et al., 2000). However, our empirical study shows that no criterion consistently performs better than the others, though they all aim to balance model complexity and model goodness of fit. In practice, we advocate combining resulting from several information criteria, utilizing domain knowledge, and examining the clustering patterns with varying number of clusters to reach conclusions. To obtain the standard errors of the estimated parameters, we utilize the SEM algorithm in Meng and Rubin (1991). Details are provided in Section A.5 of the Supplementary Material.

## 4 Simulation Study

### 4.1 Simulation Setup

We simulate  $N$  samples from a MHMM- $\beta$  model with  $M$  states and  $K$  clusters. First, the QDs are randomly allocated to different clusters with assignment probabilities  $\delta_k, k \in \{1, \dots, K\}$ , where  $\sum_{k=1}^K \delta_k = 1$ . For each dot in cluster  $k$ , we generate its hidden-state sequence as a Markov chain, with the transition matrix  $\mathbf{\Pi}_k, k \in \{1, \dots, K\}$ . We then simulate the intensities given the hidden state sequence by sampling from the inflated-Beta distribution with parameters  $(a_h, b_h, \epsilon_h^{(0)}, \epsilon_h^{(1)}), h \in \{1, \dots, M\}$ .

Here we mainly present simulation settings that mimic the QD application. The total number of dots  $N \in \{50, 100\}$ , and the number of states and clusters are fixed to be 3, i.e.,  $M = K = 3$ . The cluster probabilities  $(\delta_1, \delta_2, \delta_3)$  have two scenarios: a relatively balanced partition  $(0.3, 0.3, 0.4)$  and an unbalanced partition  $(0.7, 0.2, 0.1)$ . The transition matrices

are given by

$$\mathbf{\Pi}_1 = \begin{bmatrix} 0.50 & 0.25 & 0.25 \\ 0.25 & 0.50 & 0.25 \\ 0.25 & 0.25 & 0.50 \end{bmatrix}, \mathbf{\Pi}_2 = \begin{bmatrix} 0.94 & 0.05 & 0.01 \\ 0.01 & 0.92 & 0.07 \\ 0.01 & 0.05 & 0.94 \end{bmatrix}, \mathbf{\Pi}_3 = \begin{bmatrix} 0.84 & 0.12 & 0.04 \\ 0.06 & 0.73 & 0.21 \\ 0.02 & 0.17 & 0.81 \end{bmatrix}$$

The parameters for each state are also set as follows:  $(a_1, b_1, \epsilon_1^{(0)}, \epsilon_1^{(1)}) = (2, 4, 0.1, 0.1)$ ,  $(a_2, b_2, \epsilon_2^{(0)}, \epsilon_2^{(1)}) = (8, 4, 0.05, 0.05)$ , and  $(a_3, b_3, \epsilon_3^{(0)}, \epsilon_3^{(1)}) = (10, 2, 0.01, 0.01)$ .

## 4.2 Competing Methods

We compare our proposed mixture hidden Markov model with inflated Beta distribution, denoted by MHMM- $\beta$ , to its closest competitor, the Gaussian mixture HMM model, denoted as MHMM-G. We also include an oracle procedure, denoted as MHMM- $\beta^*$ , as a benchmark, where the clustering information is assumed known.

## 4.3 Evaluation Metrics

We report the estimation error of the inflated Beta distributions with  $\text{Er}(\widehat{\boldsymbol{\theta}}) = \sum_{h=1}^M \text{Er}(\widehat{\boldsymbol{\theta}}_h)$ , where  $\text{Er}(\widehat{\boldsymbol{\theta}}_h) = \|\widehat{\boldsymbol{\theta}}_h - \boldsymbol{\theta}_h\|_2$ , with  $\widehat{\boldsymbol{\theta}}_h = (\widehat{a}_h, \widehat{b}_h, \widehat{\epsilon}_h^{(0)}, \widehat{\epsilon}_h^{(1)})^\top$  and  $\boldsymbol{\theta}_h = (a_h, b_h, \epsilon_h^{(0)}, \epsilon_h^{(1)})^\top$  representing the estimated and true parameters for state  $h$ . Similarly, the estimation error of the transition matrices is  $\text{Er}(\widehat{\mathbf{\Pi}}) = \sum_{k=1}^K \text{Er}(\widehat{\mathbf{\Pi}}_k)$ , where  $\text{Er}(\widehat{\mathbf{\Pi}}_k) = \|\widehat{\mathbf{\Pi}}_k - \mathbf{\Pi}_k\|_F$ , with  $\widehat{\mathbf{\Pi}}_k$  and  $\mathbf{\Pi}_k$  representing the estimated and true transition matrix for cluster  $k$ , respectively. To measure the accuracy of retrieving the true cluster pattern of the dots, we report the percentage of correct clustering:  $\text{CC} = \sum_{i=1}^N I(\widehat{\mathbf{z}}_i = \mathbf{z}_i)/N$ . The simulation under each setting is replicated 100 times and the results are averaged.

## 4.4 Simulation Results

The simulation results, presented in Tables 2 and 3, evaluate the performance of the proposed MHMM- $\beta$  model and its close competitor under balanced and unbalanced cluster settings, across varying sample sizes ( $N$ ) and time series lengths ( $T$ ). Also, the oracle MHMM- $\beta^*$  bypasses the clustering step and achieves the lowest parameter estimation errors, which serves as a benchmark for the achievable accuracy.

In the balanced cluster setting (Table 2), the proposed MHMM- $\beta$  consistently outperforms the competing method in terms of clustering accuracy (CC), achieving rates close to or exceeding 96% across all scenarios. The clustering performance of MHMM-G is significantly lower, with CC values around 30-36%, underscoring the benefit of using the inflated Beta distribution for modeling bounded intensities with inflation at 0 and 1. The estimation errors of MHMM- $\beta$  are only slightly higher compared to the oracle method MHMM- $\beta^*$ , as expected. Increasing the sample size ( $N$ ) and time series length ( $T$ ) generally leads to improved parameter estimation, reflecting the efficiency of the proposed method in utilizing larger data.

In the unbalanced cluster setting (Table 3), the clustering accuracy (CC) of MHMM- $\beta$  remains strong, ranging from 81% to 85%. The estimation errors for both transition matrices and state parameters are slightly higher than in the balanced setting. Nonetheless, the MHMM- $\beta$  model consistently outperforms MHMM-G.

These results underscore the effectiveness of the MHMM- $\beta$  model in accurately capturing both the state dynamics and the clustering structure of the QD intensities, making it a powerful tool for integrative analysis in complex scenarios.



Table 2: Simulation: Results under the balanced settings.

Method	Length ( $T$ )	$\text{Er}(\hat{\boldsymbol{\theta}})$	$\text{Er}(\hat{\boldsymbol{\Pi}})$	CC
Sample size ( $N$ ) = 50				
MHMM- $\beta^*$	1000	0.56 (0.03)	0.17 (0.00)	
MHMM-G			0.98 (0.01)	0.36 (0.01)
MHMM- $\beta$		1.56 (0.11)	0.32 (0.02)	0.96 (0.01)
Sample size ( $N$ ) = 50				
MHMM- $\beta^*$	2000	0.52 (0.04)	0.17 (0.00)	
MHMM-G			0.97 (0.01)	0.31 (0.00)
MHMM- $\beta$		1.66 (0.13)	0.28 (0.02)	0.98 (0.01)
Sample size ( $N$ ) = 100				
MHMM- $\beta^*$	1000	0.54 (0.03)	0.17 (0.00)	
MHMM-G			0.97 (0.01)	0.33 (0.00)
MHMM- $\beta$		1.46 (0.13)	0.26 (0.02)	0.98 (0.01)
Sample size ( $N$ ) = 100				
MHMM- $\beta^*$	2000	0.50 (0.03)	0.16 (0.00)	
MHMM-G			0.97 (0.01)	0.31 (0.00)
MHMM- $\beta$		1.48 (0.12)	0.27 (0.02)	0.98 (0.01)

Table 3: Simulation: Results under the unbalanced settings.

Method	Length ( $T$ )	$\text{Er}(\hat{\boldsymbol{\Theta}})$	$\text{Er}(\hat{\boldsymbol{\Pi}})$	CC
Sample size ( $N$ ) = 50				
MHMM- $\beta^*$	1000	0.78 (0.04)	0.18 (0.00)	
MHMM-G			1.22 (0.02)	0.59 (0.01)
MHMM- $\beta$		1.08 (0.08)	0.59 (0.02)	0.81 (0.01)
Sample size ( $N$ ) = 50				
MHMM- $\beta^*$	2000	0.67 (0.03)	0.17 (0.00)	
MHMM-G			1.24 (0.02)	0.57 (0.01)
MHMM- $\beta$		1.02 (0.08)	0.54 (0.03)	0.85 (0.01)
Sample size ( $N$ ) = 100				
MHMM- $\beta^*$	1000	0.77 (0.04)	0.17 (0.00)	
MHMM-G			1.21 (0.02)	0.59 (0.01)
MHMM- $\beta$		1.25 (0.11)	0.58 (0.03)	0.82 (0.02)
Sample size ( $N$ ) = 100				
MHMM- $\beta^*$	2000	0.74 (0.04)	0.16 (0.00)	
MHMM-G			1.22 (0.02)	0.58 (0.01)
MHMM- $\beta$		1.16 (0.12)	0.56 (0.03)	0.84 (0.02)

## 5 Case Study: Integrative Analysis of Multiple Quantum Dots

We applied the proposed method to analyze the quantum dot data described in Section 2. Chemists believe that these quantum dots may transit between up to 3 states, corresponding to relatively low, median, and high levels of intensity of emitting photons under continuous excitation. Owing to the denosing and standardization procedure, all the dots became comparable. Thus, our main interests were to identify the three intensity states across all quantum dots, and examine cluster patterns of quantum dots with unique transition behaviors across intensity states; in particular, we hope to verify that the dots could exhibit either “blinking” or “flickering” styles of intensity fluctuations.

### 5.1 Cluster Patterns

We applied the proposed MHMM- $\beta$  approach with varying number of clusters. The cluster patterns are displayed in Figure 4, in which the colors or the grey levels represent different clusters and the stripes show how the dots are put into more and more clusters from the left to the right.

Starting from the 2-cluster model, it can be seen that in the 3-cluster model the third cluster is formed by QDs from both clusters. From then on, when the number of clusters increases, the new clusters are mainly from further splitting the third cluster, and the first two clusters remain relatively stable throughout. This clear pattern suggests that the 3-cluster model is the most stable and informative. We have also computed BIC and ICL values for these models and unfortunately they had a big discrepancy: BIC would select the 6-cluster model while ICC suggested 1 or 2 clusters. This in fact is consistent with comparative studies in the literature, which have shown that when the clusters are too overlapped, ICL tends to favor less number of clusters than BIC. From these results and after consulting with our chemistry collaborators, we decided to mainly focus on the results from the three-cluster

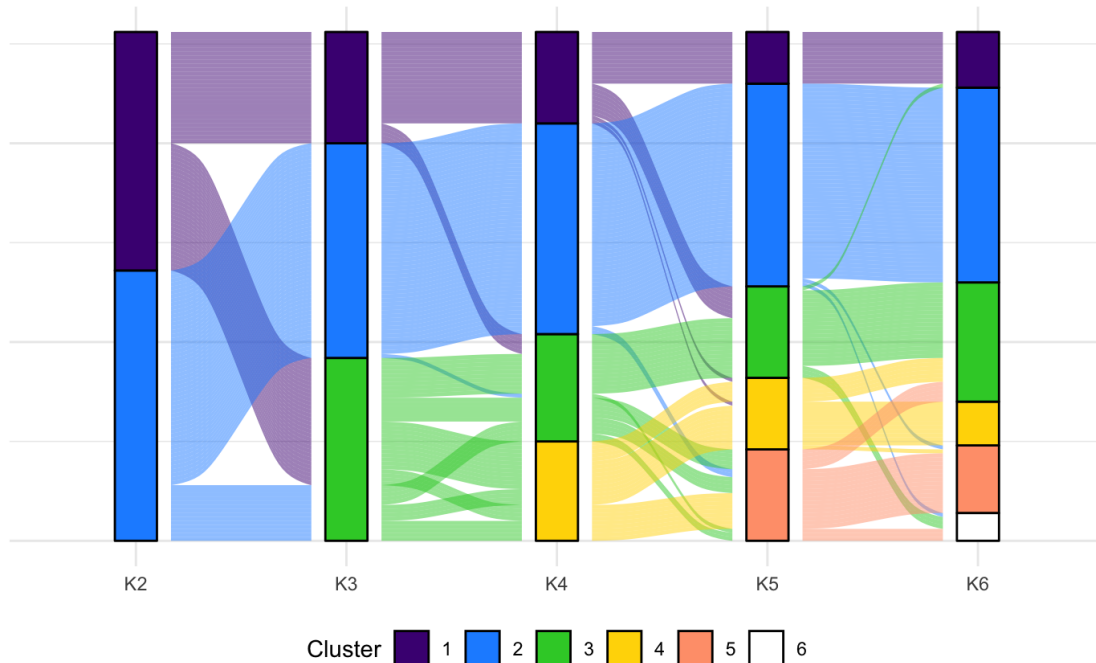


Figure 4: Quantum dot analysis: Cluster patterns.

model; as to be shown below, the results indeed are highly interpretable based on principles of chemistry and physics. We also provide the results from other models in Section B of the Supplementary Material.

## 5.2 Results from 3-Cluster Model

In Figure 5, the right panel shows the estimated 0/1 inflated Beta distributions of the three intensity states from the MHMM- $\beta$  model. With the estimated state series, we also computed the empirical distributions of the three states directly from the standardized intensity data, which are shown in the left panel. As expected, the estimated and the empirical distributions are quite similar to each other, suggesting that there are no apparent outliers and the MHMM- $\beta$  model fits the data well and successfully captured the collective behaviors of intensity fluctuations of all QDs.

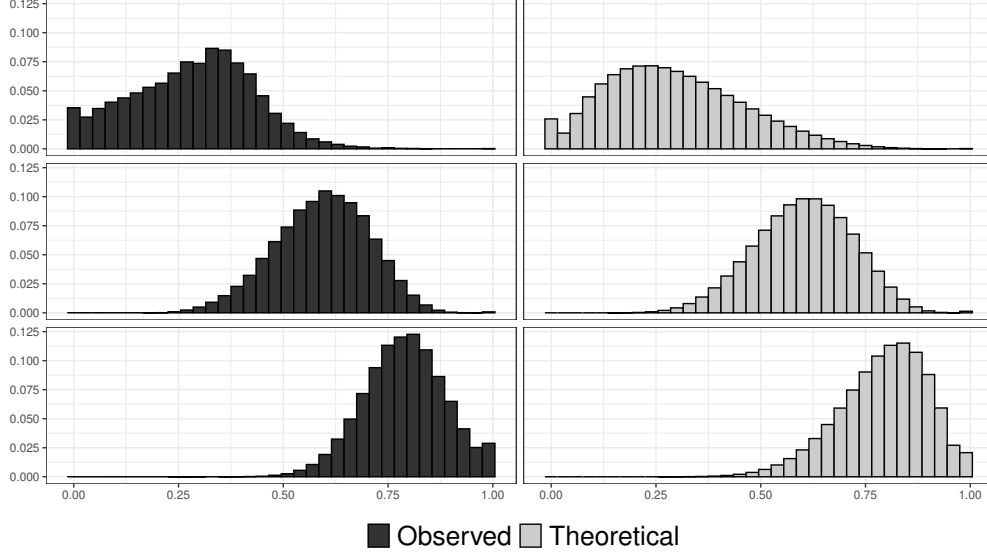


Figure 5: Quantum dot analysis: Comparison of the three intensity states.

Table 4 reports the estimation results. Besides the parameter estimates from the inflated Beta distributions, we also report the estimated mean and variance of each distribution, where

$$\begin{aligned}\hat{\mu}_h &= \hat{a}_h / (\hat{a}_h + \hat{b}_h) + \hat{\epsilon}_h^{(1)}, \\ \hat{\sigma}_h^2 &= (1 - \hat{\epsilon}_h^{(0)} - \hat{\epsilon}_h^{(1)}) \frac{(\hat{a}_h^3 + \hat{a}_h^2 \hat{b}_h + \hat{a}_h^2 + \hat{a}_h \hat{b}_h)}{(\hat{a}_h + \hat{b}_h)^2 (\hat{a}_h + \hat{b}_h + 1)} + \hat{\epsilon}_h^{(1)},\end{aligned}$$

for  $h = 1, \dots, 3$ . As seen from both Figure 5 and the estimated parameters in Table 4, the three states clearly correspond to relatively low, medium, and high intensity levels. The low-intensity state (State 1) accommodates intensities in the range of about 0.00 to 0.50, with mean 0.290 and relatively the highest variance. The medium-intensity state (State 2) mostly concentrates within the 0.50 to 0.80 spectrum, with mean 0.597 and a relatively small variance. The high-intensity state (State 3) covers the range of about 0.75 to 1.00, with mean 0.787 and relatively the smallest variance. The zero and one inflation rates are also reflected in Figure 5. The low-intensity state accommodates the zero intensities, while the high-intensity state encompasses all the intensities elevated to one.

Table 4: Quantum dot analysis: Estimated parameters of the fitted 3-cluster MHMM- $\beta$  model.

	State 1	State 2	State 3
$\hat{\epsilon}^{(0)}$	0.025 ( $1.163 \times 10^{-3}$ )	0.000 ( $5.742 \times 10^{-6}$ )	0.000 ( $1.145 \times 10^{-13}$ )
$\hat{\epsilon}^{(1)}$	0.000 ( $1.521 \times 10^{-6}$ )	0.001 ( $4.091 \times 10^{-3}$ )	0.017 ( $4.803 \times 10^{-6}$ )
$\hat{a}$	2.195 ( $1.900 \times 10^{-2}$ )	10.077 ( $2.437 \times 10^{-4}$ )	11.658 ( $2.656 \times 10^{-3}$ )
$\hat{b}$	5.183 ( $4.06 \times 10^{-2}$ )	6.805 ( $6.239 \times 10^{-5}$ )	3.227 ( $1.340 \times 10^{-3}$ )
Mean	0.290	0.597	0.787
Variance	0.0266	0.0137	0.0113

### 5.3 State Transition Patterns and Clusters of Quantum Dots

The estimated transition matrices for the three clusters are as follows:

$$\hat{\mathbf{\Pi}}_1 = \begin{bmatrix} 0.848 & 0.127 & 0.025 \\ 0.060 & 0.794 & 0.146 \\ 0.017 & 0.186 & 0.796 \end{bmatrix}, \hat{\mathbf{\Pi}}_2 = \begin{bmatrix} 0.795 & 0.205 & 0.000 \\ 0.000 & 0.994 & 0.006 \\ 0.000 & 0.001 & 0.999 \end{bmatrix}, \hat{\mathbf{\Pi}}_3 = \begin{bmatrix} 0.938 & 0.057 & 0.005 \\ 0.013 & 0.924 & 0.063 \\ 0.001 & 0.067 & 0.932 \end{bmatrix}.$$

The corresponding stationary distributions from these estimated transition matrices are as follows:

$$\hat{\boldsymbol{\pi}}_1 = \begin{bmatrix} 0.213 & 0.443 & 0.344 \end{bmatrix}, \hat{\boldsymbol{\pi}}_2 = \begin{bmatrix} 0.000 & 0.089 & 0.911 \end{bmatrix}, \hat{\boldsymbol{\pi}}_3 = \begin{bmatrix} 0.106 & 0.459 & 0.435 \end{bmatrix}.$$

Based on the estimated MHMM- $\beta$  model and according to the Bayes rule, there are 28, 54, and 46 QDs in Clusters 1, 2, and 3, respectively. To visualize, we randomly pick 3 dots from each cluster and presented their intensity series along with their estimated state series in Figures 6, 7, and 8, respectively.

In Cluster 1, the QDs exhibit about 80%-85% chance of remaining at the same state and display relatively more frequent transitions between states comparing to QDs in the other two clusters. Specifically, the most frequent transitions happen from low to medium, medium to high, and high to medium, and the chances are 12.7%, 14.6%, and 18.6%, respectively. From the stationary distribution, these QDs spend relatively even amount of time in the

three states, i.e., 21.3%, 44.3%, and 34.4%, respectively. These behaviors are consistent with the examples visualized in Figure 6.

In Cluster 2, the QDs exhibit extremely high probabilities of staying in the medium or high-intensity states, and more importantly, the probabilities of transiting into the low-intensity state are essentially zero. This results in a stationary distribution showing that these QDs spend most of their time in the high-intensity state with probability 91.1%, a much smaller amount of time in the medium-intensity state with probability 8.9%, and ultimately no time at all in the low-intensity state. In Figure 7, the three randomly selected QDs from this cluster all stayed in the high-intensity state throughout the continuous excitation.

In Cluster 3, the QDs exhibit relatively high chance of remaining at the same state (92.2% - 93.8%) and display relatively less frequent transitions between states, comparing to QDs in Cluster 1. The most frequent transitions remains the same as in Cluster 1, i.e., from low to medium, medium to high, and high to medium, but the chances are reduced to 5.7%, 6.3%, and 6.7%, respectively. Consequently, the stationary distribution reveals that these QDs spend about 45% of time in either median and high-intensity states and only 10% of the time in the low-intensity state. These are reflected in Figure 8, in which two dots only spent time in median and high-intensity states while the third dot also briefly visited the low-intensity state.

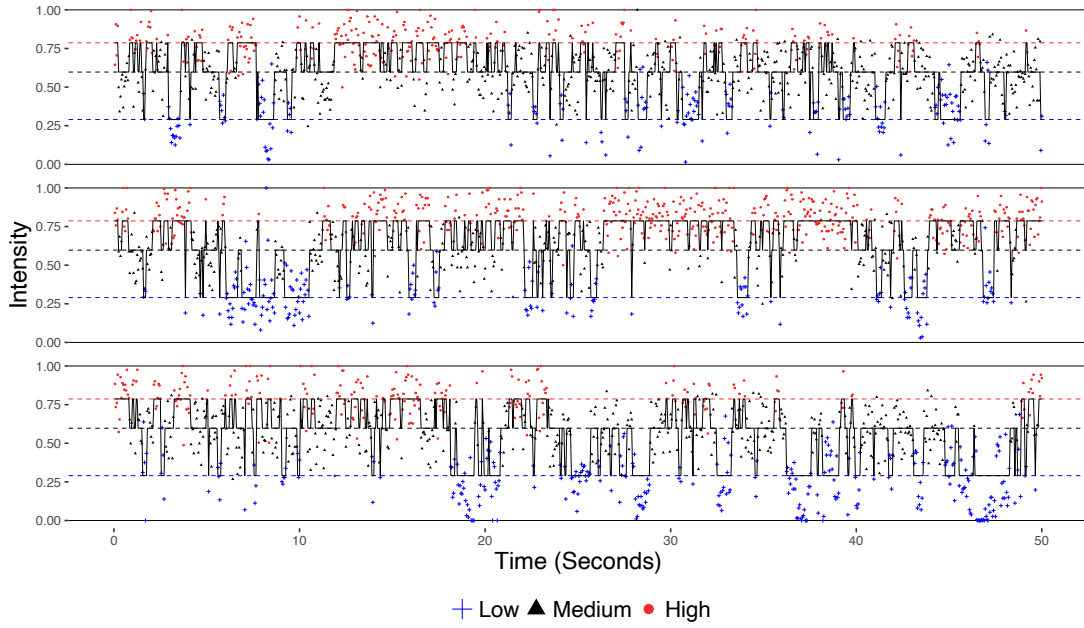


Figure 6: Quantum dot analysis: Intensity series of 3 randomly selected quantum dots in Cluster 1.

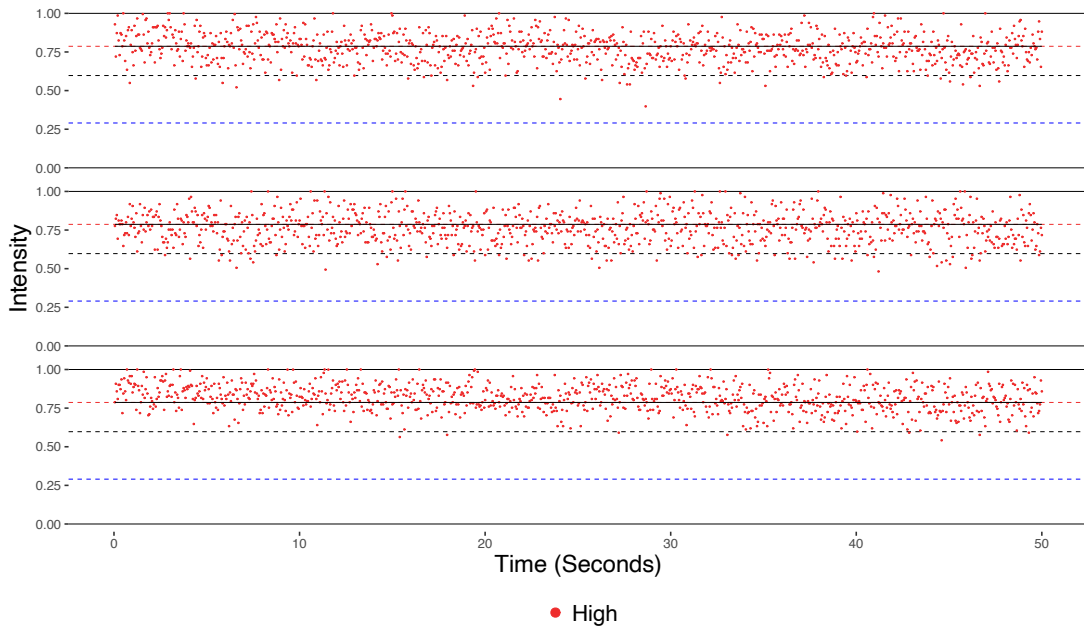


Figure 7: Quantum dot analysis: Intensity series of 3 randomly selected quantum dots in Cluster 2.

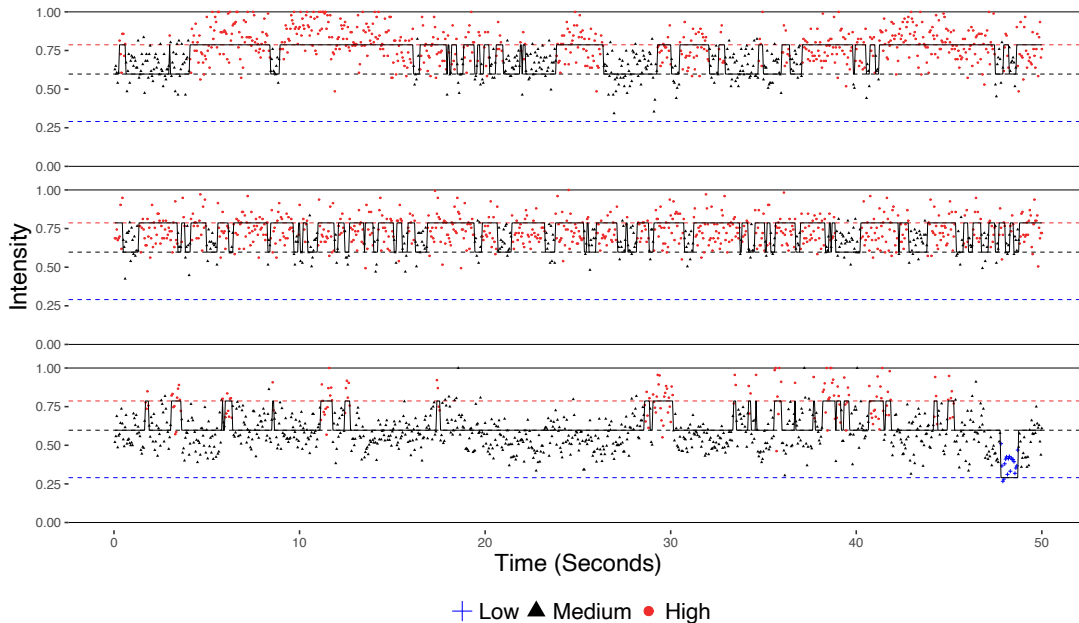


Figure 8: Quantum dot analysis: Intensity series of 3 randomly selected quantum dots in Cluster 3.

## 5.4 Implications

The analysis of quantum dot data using the proposed MHMM- $\beta$  model revealed critical insights into the intensity fluctuation behaviors and clustering patterns of QDs under continuous excitation. Specifically, three distinct clusters were identified, each characterized by unique transition dynamics and stationary distributions of intensity states. Cluster 1 exhibited relatively balanced transitions across all intensity states, with QDs spending comparable time in low, medium, and high-intensity states. Cluster 2 represented highly stable QDs predominantly residing in the high-intensity state, exhibiting minimal transitions and no time in the low-intensity state. Cluster 3 showcased QDs with moderate transition dynamics, spending most of their time in medium and high-intensity states and only briefly visiting the low-intensity state. These findings align with the hypothesized “blinking” and “flickering” styles of intensity fluctuations and provide a rigorous statistical characterization of QD behaviors, offering valuable insights for their applications in chemistry and materials science.



## 6 Conclusion & Discussion

This study introduces a novel statistical approach to analyzing the intensity fluctuation patterns of colloidal quantum dots (QDs), a critical problem in the fields of chemistry and materials science. The main challenge lies in the inherent complexity of the data: the intensity measurements exhibit intricate patterns influenced by unobserved states and are subject to substantial variation across individual QDs. The proposed mixture hidden Markov model with an inflated Beta distribution (MHMM- $\beta$ ) addresses these challenges by simultaneously modeling the intensity fluctuations and clustering the QDs based on their transition dynamics. This integrative approach captures the shared structure among QDs while allowing for individual differences, providing a more comprehensive understanding of their individual and collective behaviors under continuous excitation.

The findings from our analysis highlight the method’s effectiveness and its ability to generate interpretable results that align with principles of chemistry and physics. By identifying three distinct clusters of QDs, each characterized by unique transition dynamics and stationary distributions, our approach provides chemists with valuable insights into the interplay between QD intensity states and their fluctuation styles. These results not only validate the utility of the proposed method but also demonstrate its potential to guide future research and applications of QDs.

Looking ahead, there are several promising directions for extending this work. One critical avenue is the joint analysis of photon lifetime and intensity. Recent chemical studies have emphasized the importance of understanding the relationship between photon lifetime, which reflects aspects of the QD microenvironment, and intensity fluctuations, which capture macroenvironmental behaviors. Developing methods that incorporate photon lifetime into the integrative analysis would enable us to reveal dependencies and connections between these two dimensions, offering a more holistic view of QD properties.

Further methodological advancements could focus on developing more efficient algorithms for computation and implementing more accurate methods for model selection, particularly

for determining the optimal number of clusters. Relaxing the assumptions of shared state distributions across clusters could allow for greater flexibility in modeling. Additionally, exploring Bayesian frameworks for parameter estimation and uncertainty quantification may enhance the robustness and interpretability of the results. From a broader perspective, the proposed approach could be adapted to address other scientific problems involving complex temporal data with state-dependent dynamics. For example, similar methods could be applied in neuroimaging to study brain activity patterns or in ecology to analyze animal movement behaviors.

## Acknowledgment

Zhao and Chen were partially supported by NSF Grant CHE-2203854.

## References

- Abramowitz, M. and I. A. Stegun (1964). *Handbook of Mathematical Functions with Formulas, Graphs, and Mathematical Tables* (Tenth Edition ed.). New York.
- Akaike, H. (1974). A new look at the statistical model identification. *IEEE Transactions on Automatic Control* 19, 716–723.
- Biernacki, C., G. Celeux, and G. Govaert (2000). Assessing a mixture model for clustering with the integrated completed likelihood. *IEEE Transactions on Pattern Analysis and Machine Intelligence* 22(7), 719–725.
- Bruns, O. T., T. S. Bischof, D. K. Harris, D. Franke, Y. Shi, L. Riedemann, A. Bartelt, F. B. Jaworski, J. A. Carr, C. J. Rowlands, M. W. B. Wilson, O. Chen, H. Wei, G. W. Hwang, D. M. Montana, I. Coropceanu, O. B. Achorn, J. Kloepper, J. Heeren, P. T. C. So, D. Fukumura, K. F. Jensen, R. K. Jain, and M. G. Bawendi (2017, 4). Next-generation

- in vivo optical imaging with short-wave infrared quantum dots. *Nature Biomedical Engineering* 1(4).
- Deb, P., W. T. Gallo, P. Ayyagari, J. M. Fletcher, and J. L. Sindelar (2011). The effect of job loss on overweight and drinking. *Journal of Health Economics* 30(2), 317–327.
- Deb, P. and P. K. Trivedi (1997). Demand for medical care by the elderly: A finite mixture approach. *Journal of Applied Econometrics* 12(3), 313–336.
- Dempster, A. P., N. M. Laird, and D. B. Rubin (1977). Maximum likelihood from incomplete data via the EM algorithm. *Journal of the Royal Statistical Society: Series B (Methodological)* 39(1), 1–22.
- Dias, J. G., J. K. Vermunt, and S. Ramos (2010). Mixture hidden markov models in finance research. In *Advances in Data Analysis, Data Handling and Business Intelligence*, pp. 451–459. Springer.
- Efros, A. L. and M. Rosen (1997, Feb). Random telegraph signal in the photoluminescence intensity of a single quantum dot. *Physical Review Letters* 78, 1110–1113.
- Fahey, M., P. Ferrari, N. Slimani, J. Vermunt, I. White, K. Hoffmann, E. Wirfält, C. Bamia, M. Touvier, J. Linseisen, M. Rodriguez-Barranco, R. Tumino, E. Lund, K. Overvad, H. Bueno-de Mesquita, S. Bingham, and E. Riboli (2011, 08). Identifying dietary patterns using a normal mixture model: Application to the epic study. *Journal of Epidemiology and Community Health* 66, 89–94.
- Frantsuzov, P., M. Kuno, B. Jankó, and R. A. Marcus (2008, July). Universal emission intermittency in quantum dots, nanorods and nanowires. *Nature Physics* 4(7), 519–522.
- Kuno, M., D. P. Fromm, H. F. Hamann, A. Gallagher, and D. J. Nesbitt (2000, 02). Nonexponential “blinking” kinetics of single CdSe quantum dots: A universal power law behavior. *The Journal of Chemical Physics* 112(7), 3117–3120.

- Li, X., Y. Zhao, F. Fan, L. Levina, M. Liu, R. Quintero-Bermudez, X. Gong, L. Quan, J. Fan, Z. Yang, S. Hoogland, O. Voznyy, and Lu (2018). Bright colloidal quantum dot light-emitting diodes enabled by efficient chlorination. *Nature Photonics* *12*(3), 159–164.
- Magde, D., E. Elson, and W. W. Webb (1972, Sep). Thermodynamic fluctuations in a reacting system—measurement by fluorescence correlation spectroscopy. *Physical Review Letters* *29*, 705–708.
- McKinney, S. A., C. Joo, and T. Ha (2006a). Analysis of single-molecule fret trajectories using hidden markov modeling. *Biophysical Journal* *91*(5), 1941–1951.
- McKinney, S. A., C. Joo, and T. Ha (2006b). Analysis of single-molecule fret trajectories using hidden markov modeling. *Biophysical Journal* *91*(5), 1941–1951.
- Meng, X.-L. and D. B. Rubin (1991). Using em to obtain asymptotic variance-covariance matrices: The sem algorithm. *Journal of the American Statistical Association* *86*(416), 899–909.
- Mücksch, J., P. Blumhardt, M. T. Strauss, E. P. Petrov, R. Jungmann, and P. Schuille (2018). Quantifying reversible surface binding via surface-integrated fluorescence correlation spectroscopy. *Nano Letters* *18*(5), 3185–3192.
- Nirmal, M., B. O. Dabbousi, M. G. Bawendi, J. J. Macklin, J. K. Trautman, T. D. Harris, and L. E. Brus (1996, 10). Fluorescence intermittency in single cadmium selenide nanocrystals. *Nature* *383*(6603), 802–804.
- Pirchi, M., R. Tsukanov, R. Khamis, T. E. Tomov, Y. Berger, D. C. Khara, H. Volkov, G. Haran, and E. Nir (2016). Photon-by-photon hidden markov model analysis for microsecond single-molecule fret kinetics. *The Journal of Physical Chemistry B* *120*(51), 13065–13075.

- Protesescu, L., S. Yakunin, M. I. Bodnarchuk, F. Krieg, R. Caputo, C. H. Hendon, R. X. Yang, A. Walsh, and M. V. Kovalenko (2015). Nanocrystals of cesium lead halide perovskites (cspb $x$ 3,  $x = \text{cl, br, and i}$ ): Novel optoelectronic materials showing bright emission with wide color gamut. *Nano Letters* 15(6), 3692–3696. PMID: 25633588.
- Rabiner, L. (1989). A tutorial on hidden markov models and selected applications in speech recognition. *Proceedings of the IEEE* 77(2), 257–286.
- Schlattmann, P. and D. Böhning (1993). Mixture models and disease mapping. *Statistics in Medicine* 12(19-20), 1943–1950.
- Schwarz, G. (1978). Estimating the Dimension of a Model. *The Annals of Statistics* 6(2), 461–464.
- Sisamakris, E., A. Valeri, S. Kalinin, P. J. Rothwell, and C. A. M. Seidel (2010). Accurate single-molecule fret studies using multiparameter fluorescence detection. *Methods in Enzymology* 475, 455–514.
- Steinley, D. and M. Brusco (2011, 02). Evaluating mixture modeling for clustering: Recommendations and cautions. *Psychological methods* 16, 63–79.
- Wang, M., S. Abdelfattah, N. Moustafa, and J. Hu (2018). Deep gaussian mixture-hidden markov model for classification of eeg signals. *IEEE Transactions on Emerging Topics in Computational Intelligence* 2(4), 278–287.

# Supplementary Material

## A Computation Details

### A.1 Derivation of the likelihood functions

The forward probabilities are defined as

$$\alpha_{i,t,k,h} = P[(x_{i,1}, \dots, x_{i,t})^\top, s_{i,t,h} = 1 \mid z_{i,k} = 1, \Theta^{(j)}].$$

Then  $\alpha_{i,T,k,h}$ , where  $T$  denotes the last time point in a sequence, stands for the likelihood of hidden state sequence ending in state  $h$ . That is, all the hidden sequences of dot  $i$  ending with state  $h$  are considered. So, we can sum up  $\alpha_{i,T,k,h}$  w.r.t.  $h = \{1, \dots, M\}$  to get the summation over all possible sequences in (3).

The complete-data log-likelihood function is given by:

$$\begin{aligned} l(\Theta; \mathbf{X}, \mathbf{S}, \mathbf{Z}) &= \sum_{i=1}^N \log \left\{ \prod_{k=1}^K [\delta_k \boldsymbol{\pi}_{k, \mathbf{s}_{i,1}} f(x_{i,1} \mid \mathbf{s}_{i,1}) \prod_{t=2}^T (\boldsymbol{\Pi}_k)_{\mathbf{s}_{i,t-1}, \mathbf{s}_{i,t}} f(x_{i,t} \mid \mathbf{s}_{i,t})]^{I(z_{i,k}=1)} \right\} \\ &= \sum_{i=1}^N \sum_{k=1}^K I(z_{i,k} = 1) \log(\delta_k) + \sum_{i=1}^N \sum_{k=1}^K I(z_{i,k} = 1) \sum_{p=1}^M I(s_{i,1,p} = 1) \log(\boldsymbol{\pi}_{k,p}) \\ &\quad + \sum_{i=1}^N \sum_{k=1}^K I(z_{i,k} = 1) \log \left( \prod_{t=2}^T (\boldsymbol{\Pi}_k)_{\mathbf{s}_{i,t-1}, \mathbf{s}_{i,t}} \right) + \sum_{i=1}^N \sum_{k=1}^K I(z_{i,k} = 1) \log \left( \prod_{t=1}^T f(x_{i,t} \mid \mathbf{s}_{i,t}) \right) \\ &= \sum_{i=1}^N \sum_{k=1}^K I(z_{i,k} = 1) \log(\delta_k) + \sum_{i=1}^N \sum_{k=1}^K I(z_{i,k} = 1) \sum_{p=1}^M I(s_{i,1,p} = 1) \log(\boldsymbol{\pi}_{k,p}) \\ &\quad + \sum_{i=1}^N \sum_{k=1}^K I(z_{i,k} = 1) \left\{ \sum_{t=2}^T \sum_{p=1}^M \sum_{q=1}^M I(s_{i,t-1,p} = 1, s_{i,t,q} = 1) \log((\boldsymbol{\Pi}_k)_{p,q}) \right\} \\ &\quad + \sum_{i=1}^N \sum_{k=1}^K I(z_{i,k} = 1) \left\{ \sum_{t=1}^T \sum_{p=1}^M I(s_{i,t,p} = 1) \log(f(x_{i,t} \mid s_{i,t,p} = 1)) \right\}. \end{aligned} \tag{7}$$

## A.2 E-Step

Let  $\Theta^{(j)}$  denote the set of parameter estimates from  $j^{\text{th}}$  iteration. Let

$$\begin{aligned} Q(\Theta \mid \Theta^{(j)}) &= E_{(\mathbf{S}, \mathbf{Z}) \sim p(\cdot, \cdot \mid \mathbf{X}, \Theta^{(j)})} [l(\Theta; \mathbf{X}, \mathbf{S}, \mathbf{Z}) \mid \mathbf{X}, \Theta^{(j)}] \\ &= E_{\mathbf{S} \sim p(\cdot \mid \mathbf{X}, \mathbf{Z}, \Theta^{(j)})} \{ E_{\mathbf{Z} \sim p(\cdot \mid \mathbf{X}, \Theta^{(j)})} [l(\Theta; \mathbf{X}, \mathbf{S}, \mathbf{Z})] \}. \end{aligned} \quad (8)$$

In (8), we rewrite the integration w.r.t. the joint distribution  $(\mathbf{S}, \mathbf{Z})$  into a double-expectation structure, which could simplify the computation. For each dot  $i$ , given the observed intensities and parameters  $\Theta^{(j)}$ , we will present the formula for all unknown values in (5).

(i) Compute  $I(z_{i,k} = 1)$ :

$$\begin{aligned} E[I(z_{i,k} = 1) \mid \mathbf{x}_i, \Theta^{(j)}] &= Pr(z_{i,k} = 1 \mid \mathbf{x}_i, \Theta^{(j)}) \\ &= \frac{Pr(z_{i,k} = 1, \mathbf{x}_i \mid \Theta^{(j)})}{\sum_{k'=1, \dots, K} Pr(z_{i,k'} = 1, \mathbf{x}_i \mid \Theta^{(j)})} \end{aligned} \quad (9)$$

Within formula (9), the key part is  $Pr(z_{i,k} = 1, \mathbf{x}_i \mid \Theta^{(j)})$ . To calculate this probability, we adopt the idea of forward-backward algorithm in dynamic programming (Rabiner, 1989).

That is

$$\alpha_{i,t,k,h} = Pr((x_{i,1}, \dots, x_{i,t})^T, s_{i,t,h} = 1 \mid z_{i,k} = 1, \Theta^{(j)}) \quad (10)$$

The value of  $\alpha_{i,t,k}$  can be determined through iterative computation (11).

$$\begin{aligned} \alpha_{i,t,k} &= \boldsymbol{\pi}_k \circ (f(x_{i,t}) \mid s_{i,t,h} = 1, \Theta^{(j)})_{h=1, \dots, M}^T, \text{ when } t = 1, \\ \alpha_{i,t,k} &= (\mathbf{\Pi}_k^T \cdot \alpha_{i,t-1,k}) \circ (f(x_{i,t}) \mid s_{i,t,h} = 1, \Theta^{(j)})_{h=1, \dots, M}^T, \text{ when } t > 1, \end{aligned} \quad (11)$$

where  $\circ$  is the Hadamard product.

Using the forward probabilities at the last time point  $T$ , we have  $Pr(z_{i,k} = 1, \mathbf{x}_i \mid \Theta^{(j)}) =$

$\|\boldsymbol{\alpha}_{i,T,k}\|_1 = \sum_{h=1}^M \alpha_{i,T,k,h}$  and update (9) to (12):

$$\begin{aligned} E[I(z_{i,k} = 1) \mid \mathbf{x}_i, \boldsymbol{\Theta}^{(j)}] &= \frac{\|\boldsymbol{\alpha}_{i,T,k}\|_1}{\sum_{k'=1,\dots,K} \|\boldsymbol{\alpha}_{i,T,k'}\|_1} \\ &= \frac{\sum_{h=1}^M \alpha_{i,T,k,h}}{\sum_{k'=1,\dots,K} \sum_{h=1}^M \alpha_{i,T,k',h}}. \end{aligned} \quad (12)$$

Follow the notation from Rabiner (1989), we denote  $E[I(z_{i,k} = 1) \mid \mathbf{x}_i, \boldsymbol{\Theta}^{(j)}]$  as  $\tau_{i,k}(\boldsymbol{\Theta}^{(j)})$ .

**(ii) Compute  $I(s_{i,t,p} = 1)$  and  $I(s_{i,1,p} = 1)$  :**

Only  $E[I(s_{i,t,p} = 1)]$  is solved and  $E[I(s_{i,1,p} = 1)]$  is treated as a special case of the previous formula. Continue with (5), after solving the inner expectation, the outer expectation is:

$$\begin{aligned} E[I(s_{i,t,h} = 1) \mid \mathbf{z}_i, \mathbf{x}_i, \boldsymbol{\Theta}^{(j)}] &= Pr(s_{i,t,h} = 1 \mid \mathbf{z}_i, \mathbf{x}_i, \boldsymbol{\Theta}^{(j)}) \\ &= \frac{Pr(s_{i,t,h} = 1, \mathbf{x}_i \mid \mathbf{z}_i, \boldsymbol{\Theta}^{(j)})}{\sum_{h'=1,\dots,M} Pr(s_{i,t,h'} = 1, \mathbf{x}_i \mid \mathbf{z}_i, \boldsymbol{\Theta}^{(j)})}. \end{aligned} \quad (13)$$

Within formula (13), the key part is  $Pr(s_{i,t,h} = 1, \mathbf{x}_i \mid \mathbf{z}_i, \boldsymbol{\Theta}^{(j)})$ . To calculate this probability, we adopt the idea of backward algorithm in dynamic programming (Rabiner, 1989). Then we give the definition (14) of backward probability  $\boldsymbol{\beta}_{i,t,k} = (\beta_{i,t,k,h})_{h=1,\dots,M}^T$ , where

$$\beta_{i,t,k,h} = Pr((x_{i,t+1}, \dots, x_{i,T})^T, s_{i,t,h} = 1 \mid z_{i,k} = 1, \boldsymbol{\Theta}^{(j)}). \quad (14)$$

The value of  $\boldsymbol{\beta}_{i,t,k}$  can be determined by iterative calculation (15).

$$\begin{aligned} \boldsymbol{\beta}_{i,t,k} &= \mathbf{1}, \text{ when } t = T, \\ \boldsymbol{\beta}_{i,t,k} &= \boldsymbol{\Pi}_k^T \cdot [(f(x_{i,t}) \mid s_{i,t,h} = 1, \boldsymbol{\Theta}^{(j)})_{h=1,\dots,M} \circ \boldsymbol{\beta}_{i,t+1,k}], \text{ when } t < T. \end{aligned} \quad (15)$$

Combine the forward probabilities and backward probabilities, we have the following equa-



tion to update (13),

$$E(\mathbf{s}_{it} \mid \mathbf{z}_i, \mathbf{x}_i, \Theta^{(j)}) = Pr(\mathbf{s}_{i,t}, \mathbf{x}_i \mid \mathbf{z}_i, \Theta^{(j)}) = \frac{\boldsymbol{\alpha}_{i,t,k} \circ \boldsymbol{\beta}_{i,t,k}}{\boldsymbol{\alpha}_{i,t,k} \cdot \boldsymbol{\beta}_{i,t,k}}.$$

And then,

$$E[I(s_{i,t,h} = 1)] = \sum_{k=1}^K Pr(s_{i,t,h} = 1 \mid z_{i,k} = 1, \mathbf{x}_i, \Theta^{(j)}) Pr(z_{i,k} = 1 \mid \mathbf{x}_i, \Theta^{(j)}),$$

where all values are calculated before. Following the notations from [Rabiner \(1989\)](#), we define  $\gamma_{i,t,k,h}(\Theta^{(j)}) = E[I(s_{i,t,h} = 1) \mid z_{i,k} = 1, \mathbf{x}_i, \Theta^{(j)}]$  and  $\eta_{i,t,h}(\Theta^{(j)}) = E[I(s_{i,t,h} = 1) \mid \mathbf{x}_i, \Theta^{(j)}]$ .

(iii) Compute  $I(s_{i,t-1,p} = 1, s_{i,t,q} = 1)$ :

$$\begin{aligned} & E[I(s_{i,t-1,p} = 1, s_{i,t,q} = 1) \mid \mathbf{z}_i, \mathbf{x}_i, \Theta^{(j)}] \\ &= Pr[s_{i,t-1,p} = 1, s_{i,t,q} = 1 \mid \mathbf{z}_i, \mathbf{x}_i, \Theta^{(j)}] \\ &= \frac{\alpha_{i,t-1,k,p}(\mathbf{\Pi}_k)_{p,q} f(x_{i,t} \mid s_{i,t,q} = 1) \beta_{i,t,k,q}}{\sum_{p'=1}^M \sum_{q'=1}^M \alpha_{i,t-1,k,p'}(\mathbf{\Pi}_k)_{p',q'} f(x_{i,t} \mid s_{i,t,q'} = 1) \beta_{i,t,k,q'}}. \end{aligned} \quad (16)$$

We define  $\xi_{i,t,k,p,q}(\Theta^{(j)}) = E[I(s_{i,t-1,p} = 1, s_{i,t,q} = 1) \mid z_{i,k} = 1, \mathbf{x}_i, \Theta^{(j)}]$ .

### A.3 M-Step

The M-step will find the parameters maximizing the function  $Q(\Theta \mid \Theta^{(j)})$  which is defined using  $\tau_{i,k}(\Theta^{(j)})$ ,  $\gamma_{i,t,k,h}(\Theta^{(j)})$ ,  $\eta_{i,t,h}(\Theta^{(j)})$  and  $\xi_{i,t,k,p,q}(\Theta^{(j)})$ .

$$\begin{aligned} Q(\Theta \mid \Theta^{(j)}) &= \sum_{i=1}^N \sum_{k=1}^K \tau_{i,k}(\Theta^{(j)}) \log(\boldsymbol{\pi}_{k,s_{i,1}}) \\ &+ \sum_{i=1}^N \sum_{k=1}^K \tau_{i,k}(\Theta^{(j)}) \left\{ \sum_{t=2}^T \sum_{p=1}^M \sum_{q=1}^M \xi_{i,t,k,p,q}(\Theta^{(j)}) \log(\mathbf{\Pi}_k)_{p,q} \right\} \\ &+ \sum_{i=1}^N \sum_{k=1}^K \tau_{i,k}(\Theta^{(j)}) \left\{ \sum_{t=1}^T \sum_{p=1}^M \gamma_{i,t,k,p}(\Theta^{(j)}) \log f(x_{i,t} \mid s_{i,t,p} = 1) \right\}. \end{aligned} \quad (17)$$

**(i) Maximization with respect to  $\delta_k$ :**

Consider the parts of (18) involving  $\delta_k$ :

$$\hat{\delta}^{(j+1)} = \arg \max_{\delta} \left\{ \sum_{i=1}^N \sum_{k=1}^K \tau_{i,k}(\Theta^{(j)}) \log(\delta_k) \right\}, \quad s.t. \sum_{k=1}^K \delta_k = 1. \quad (18)$$

Use Lagrange multiplier method to maximize (18) gives us:

$$\begin{aligned} \mathcal{L} &= \sum_{i=1}^N \sum_{k=1}^K \tau_{i,k}(\Theta^{(j)}) \log(\delta_k) + \lambda \left( \sum_{k=1}^K \delta_k - 1 \right), \\ \nabla(\mathcal{L}) &= \left( \frac{\sum_{i=1}^N \tau_{i,1}(\Theta^{(j)})}{\delta_1} - \lambda, \dots, \frac{\sum_{i=1}^N \tau_{i,K}(\Theta^{(j)})}{\delta_K} - \lambda, \sum_{k=1}^K \delta_k - 1 \right)^T, \\ \text{Set } \nabla(\mathcal{L}) &= (0)_{K+1}^T, \\ \text{Solution: } \lambda &= \sum_{i=1}^N \sum_{k'=1}^K \tau_{i,k'}(\Theta^{(j)}) = N, \\ \delta_k^{(j+1)} &= \frac{\sum_{i=1}^N \tau_{i,k}(\Theta^{(j)})}{N}. \end{aligned} \quad (19)$$

**(ii) Update  $(\Pi_k)_{p,q}$ :**

Consider the parts of (18) involving  $(\Pi_k)_{p,q}$ :

$$\begin{aligned} \hat{\Pi}_k^{(j+1)} &= \arg \max_{\Pi_k} \sum_{i=1}^N \sum_{k=1}^K \tau_{i,k}(\Theta^{(j)}) \left\{ \sum_{t=2}^T \sum_{p=1}^M \sum_{q=1}^M \xi_{i,t,k,p,q}(\Theta^{(j)}) \log(\Pi_k)_{p,q} \right\}, \\ s.t. \sum_q^M (\Pi_k)_{p,q} &= 1, \quad \forall p \in \{1, \dots, M\}, k \in \{1, \dots, K\}. \end{aligned}$$

Similar to the lagrange multiplier method in (19),

$$(\Pi_k)_{p,q}^{(j+1)} = \frac{\sum_{i=1}^N \tau_{i,k}(\Theta^{(j)}) \sum_{t=2}^T \xi_{i,t,k,p,q}(\Theta^{(j)})}{\sum_{i=1}^N \tau_{i,k}(\Theta^{(j)}) \sum_{t=2}^T \sum_{q'=1}^M \xi_{i,t,k,p,q'}(\Theta^{(j)})}. \quad (20)$$

**(iii) Update  $(a_h, b_h, \epsilon_h^{(0)}, \epsilon_h^{(1)})_{h=1, \dots, M}$ :**

Consider the parts in (18) involving  $(a_h, b_h, \epsilon_h^{(0)}, \epsilon_h^{(1)})_{h=1, \dots, M}$ :

$$\begin{aligned}
(\hat{a}_h, \hat{b}_h, \hat{\epsilon}_h^{(0)}, \hat{\epsilon}_h^{(1)}) &= \arg \max_{(a_h, b_h, \epsilon_h^{(0)}, \epsilon_h^{(1)})} \sum_{i=1}^N \sum_{k=1}^K \tau_{i,k}(\Theta^{(j)}) \left\{ \sum_{t=1}^T \gamma_{i,t,k,h}(\Theta^{(j)}) \log f(x_{i,t} \mid s_{i,t,h} = 1) \right\} \\
&= \arg \max_{(a_h, b_h, \epsilon_h^{(0)}, \epsilon_h^{(1)})} \sum_{i=1}^N \sum_{k=1}^K \tau_{i,k}(\Theta^{(j)}) \left\{ \sum_{t=1}^T \gamma_{i,t,k,h}(\Theta^{(j)}) \right. \\
&\quad + [I(x_{i,t} = 0) \log(\epsilon_h^{(0)}) + I(x_{i,t} = 1) \log(\epsilon_h^{(1)}) \\
&\quad \left. + I(0 < x_{i,t} < 1) \log(1 - \epsilon_h^{(0)} - \epsilon_h^{(1)}) + I(0 < x_{i,t} < 1) \log f(x_{i,t} \mid a_h, b_h)] \right\}.
\end{aligned} \tag{21}$$

Since (21) can be separated into two parts, the  $\epsilon_h^{(0)}, \epsilon_h^{(1)}$  and the  $a_h, b_h$  can be updated separately.

**(iv) Update  $(\epsilon_h^{(0)}, \epsilon_h^{(1)})_{h=1, \dots, M}$ :**

$$\begin{aligned}
(\hat{\epsilon}_h^0, \hat{\epsilon}_h^1) &= \arg \max_{(\epsilon_h^{(0)}, \epsilon_h^{(1)})} \sum_{i=1}^N \sum_{k=1}^K \tau_{i,k}(\Theta^{(j)}) \left\{ \sum_{t=1}^T \gamma_{i,t,k,h}(\Theta^{(j)}) \right. \\
&\quad \left. [I(x_{i,t} = 0) \log(\epsilon_h^{(0)}) + I(x_{i,t} = 1) \log(\epsilon_h^{(1)}) + I(0 < x_{i,t} < 1) \log(1 - \epsilon_h^{(0)} - \epsilon_h^{(1)})] \right\}.
\end{aligned} \tag{22}$$

It is obvious the solutions to (22) are:

$$\begin{aligned}
(\epsilon_h^{(0)})^{(j+1)} &= \frac{\sum_{i=1}^N \sum_{k=1}^K \tau_{i,k}(\Theta^{(j)}) \sum_{t=1}^T \gamma_{i,t,k,h}(\Theta^{(j)}) I(x_{i,t} = 0)}{\sum_{i=1}^N \sum_{k=1}^K \tau_{i,k}(\Theta^{(j)}) \sum_{t=1}^T \gamma_{i,t,k,h}(\Theta^{(j)})}, \\
(\epsilon_h^{(1)})^{(j+1)} &= \frac{\sum_{i=1}^N \sum_{k=1}^K \tau_{i,k}(\Theta^{(j)}) \sum_{t=1}^T \gamma_{i,t,k,h}(\Theta^{(j)}) I(x_{i,t} = 1)}{\sum_{i=1}^N \sum_{k=1}^K \tau_{i,k}(\Theta^{(j)}) \sum_{t=1}^T \gamma_{i,t,k,h}(\Theta^{(j)})}.
\end{aligned}$$

**(v) Update  $(a_h, b_h)_{h=1, \dots, M}$ :**

$$(\hat{a}_h, \hat{b}_h) = \arg \max_{(a_h, b_h)} \sum_{i=1}^N \sum_{k=1}^K \tau_{i,k}(\Theta^{(j)}) \left\{ \sum_{t=1}^T \gamma_{i,t,k,h}(\Theta^{(j)}) I(0 < x_{i,t} < 1) \log(f(x_{i,t} \mid a_h, b_h)) \right\}. \tag{23}$$

We utilize the Newton-Raphson method to solve (23). In  $r^{th}$  iteration. Use  $(a_h^{(r)}, b_h^{(r)})^T$  to denote the estimates from last iteration and take derivatives of (23) and denote them as  $g_1$  and  $g_2$ :

$$\begin{aligned}
g_1 &= \frac{\partial \sum_{i=1}^N \sum_{k=1}^K \tau_{i,k}(\Theta^{(j)}) \{ \sum_{t=1}^T \gamma_{i,t,k,h}(\Theta^{(j)}) I(0 < x_{i,t} < 1) \log(f(x_{i,t} | a_h, b_h)) \}}{\partial a_h} \\
&= \sum_{i=1}^N \sum_{k=1}^K \tau_{i,k}(\Theta^{(j)}) \{ \sum_{t=1}^T \gamma_{i,t,k,h}(\Theta^{(j)}) I(0 < x_{i,t} < 1) [\psi(a_h + b_h) - \psi(a_h) + \log(x_{i,t})] \}, \\
g_2 &= \frac{\partial \sum_{i=1}^N \sum_{k=1}^K \tau_{i,k}(\Theta^{(j)}) \{ \sum_{t=1}^T \gamma_{i,t,k,h}(\Theta^{(j)}) I(0 < x_{i,t} < 1) \log(f(x_{i,t} | a_h, b_h)) \}}{\partial b_h} \\
&= \sum_{i=1}^N \sum_{k=1}^K \tau_{i,k}(\Theta^{(j)}) \{ \sum_{t=1}^T \gamma_{i,t,k,h}(\Theta^{(j)}) I(0 < x_{i,t} < 1) [\psi(a_h + b_h) - \psi(b_h) + \log(1 - x_{i,t})] \}.
\end{aligned}$$

Next, take derivatives of  $g_1$  and  $g_2$ , and denote them as  $g_{11}, g_{12}, g_{21}, g_{22}$ :

$$\begin{aligned}
g_{11} &= \frac{\partial g_1}{\partial a_h} = \sum_{i=1}^N \sum_{k=1}^K \tau_{i,k}(\Theta^{(j)}) \{ \sum_{t=1}^T \gamma_{i,t,k,h}(\Theta^{(j)}) I(0 < x_{i,t} < 1) [\psi'(a_h + b_h) - \psi'(a_h)] \}, \\
g_{12} &= \frac{\partial g_1}{\partial b_h} = \sum_{i=1}^N \sum_{k=1}^K \tau_{i,k}(\Theta^{(j)}) \{ \sum_{t=1}^T \gamma_{i,t,k,h}(\Theta^{(j)}) I(0 < x_{i,t} < 1) [\psi'(a_h + b_h)] \}, \\
g_{21} &= \frac{\partial g_2}{\partial a_h} = g_{12}, \\
g_{22} &= \frac{\partial g_2}{\partial b_h} = \sum_{i=1}^N \sum_{k=1}^K \tau_{i,k}(\Theta^{(j)}) \{ \sum_{t=1}^T \gamma_{i,t,k,h}(\Theta^{(j)}) I(0 < x_{i,t} < 1) [\psi'(a_h + b_h) - \psi'(b_h)] \}.
\end{aligned}$$

New estimates are given as follows:

$$(a_h^{(r+1)}, b_h^{(r+1)})^T = (a_h^{(r)}, b_h^{(r)})^T - \mathbf{G}^{-1} \mathbf{g},$$

where  $\mathbf{G} = \begin{pmatrix} g_{11} & g_{12} \\ g_{21} & g_{22} \end{pmatrix}$ ,  $\mathbf{g} = (g_1, g_2)^T$  and the  $\psi$  denotes the Digamma function (Abramowitz and Stegun, 1964), i.e.,  $\psi(x) = \frac{\partial}{\partial x} \ln \Gamma(x)$ .

## A.4 Pseudo-Code

The algorithms are summarized as follows.

---

**Algorithm 1** Newton-Raphson Method for  $(a_h, b_h)$

---

**Input:**  $a_h^{(j)}, b_h^{(j)}, \tau, \gamma$

Control parameters:  $\epsilon_{\text{NRtol}} = 1e - 5, \text{maxit}_{\text{NR}} = 1e + 3$

Initial values:  $a^{(0)} \leftarrow a_h^{(j)}, b^{(0)} \leftarrow b_h^{(j)}$

Initialize the temporary parameters:  $\Delta \leftarrow 1, r \leftarrow 0$

**while**  $r < \text{maxit}_{\text{NR}}$  and  $\Delta \geq \epsilon_{\text{NRtol}}$  **do**

    Calculate  $g_1, g_2, g_{11}, g_{12}, g_{21}, g_{22}$  w.r.t. (24)

    Write  $\mathbf{g}$  and  $\mathbf{G}$

$(a^{(r+1)}, b^{(r+1)})^T = (a^{(r)}, b^{(r)})^T - \mathbf{G}^{-1} \mathbf{g}$

$\Delta \leftarrow \frac{\|(a^{(r+1)} - a^{(r)}, b^{(r+1)} - b^{(r)})\|_2^2}{\|(a^{(r)}, b^{(r)})\|_2^2}$

$r \leftarrow r + 1$

**end while**

$(a_h^{(j+1)}, b_h^{(j+1)}) \leftarrow (a^{(r+1)}, b^{(r+1)})$

**Output:**  $(a_h^{(j+1)}, b_h^{(j+1)})$

---

---

**Algorithm 2** Core EM-algorithm

---

**Input:**  $\mathbf{X}$ ,  $K$ ,  $M$ ,  $N$

Set up control parameters:  $\epsilon_{\text{EM-tol}} = 1e - 5$ ,  $\text{maxit}_{\text{EM}} = 1e + 3$

Set up initial values:  $\Theta^{(0)}$

Initialize the temporary parameters:  $j \leftarrow 0$

**repeat**

▷ EM-algorithm

▷ E-step

**for**  $i = 1, \dots, N$  **do**

Using current parameters  $\Theta^{(j)}$

Calculate forward-backward probabilities,  $\alpha_{i,t,k}, \beta_{i,t,k}$

Calculate  $\tau_{i,k}(\Theta^{(j)})$ ,  $\gamma_{i,t,k,h}(\Theta^{(j)})$ ,  $\xi_{i,t,k,p,q}(\Theta^{(j)})$

**end for**

▷ M-step

**for**  $k = 1, \dots, K$  **do**

Update  $\delta_k^{(j+1)}$ .

**for**  $\forall(p, q) \in (1, \dots, M) \times (1, \dots, M)$  **do**

Update  $(\Pi_k)_{p,q}^{(j+1)}$

**end for**

**end for**

**for**  $h = 1, \dots, M$  **do**

Update  $(\epsilon_h^{(0)})^{(j+1)}$  and  $(\epsilon_h^{(1)})^{(j+1)}$

Update  $a_h^{(j+1)}, b_h^{(j+1)}$  using Algorithm 1

**end for**

$\Theta^{(j+1)}$  is the collection of all new parameters from M-step.

**until** Convergence of log-likelihood or max iteration reached.

**Output:** Estimated hidden states, cluster information, and  $\hat{\Theta}$ , the MLE of parameters.

---

## A.5 Variance Estimation

To describe the uncertainty of 0/1 inflated beta parameters, we utilize the SEM algorithm mentioned in Meng and Rubin (1991). Let  $\mathcal{F}$  be a mapping from  $\Theta$  to  $\Theta$ , such that  $\Theta^{(j+1)} = \mathcal{F}(\Theta^{(j)})$ . Moreover, the variance-covariance matrix of the parameters, denoted as  $\mathbf{V}$ , is defined and its value is given as follows:

$$\begin{aligned} \mathbf{V} &= \mathbf{I}_{oc}^{-1} + \mathbf{U}, \\ \mathbf{U} &= \mathbf{I}_{oc}^{-1} \frac{\partial \mathcal{F}}{\partial \hat{\Theta}} \left( \mathbf{I} - \frac{\partial \mathcal{F}}{\partial \hat{\Theta}} \right)^{-1}, \end{aligned} \tag{24}$$

where  $\mathbf{I}_{oc}^{-1}$  is the inverse of the observed data information matrix, and  $\frac{\partial \mathcal{F}}{\partial \Theta}$  denote the derivative of  $\mathcal{F}$  evaluated at  $\hat{\Theta}$ .

As the first key part in (24),  $\frac{\partial \mathcal{F}}{\partial \Theta}$  is calculated as follows. For simplicity, let  $m_{p,q}$  denote the  $(p, q)$ -th element of the  $\frac{\partial \mathcal{F}}{\partial \Theta}$ . To facilitate the presentation of details in SEM algorithm, we write  $\hat{\Theta}$  as a vector of length  $4M$ ,  $(\hat{\epsilon}_h^{(0)}, \hat{\epsilon}_h^{(1)}, \hat{a}_h, \hat{b}_h)_{h=1, \dots, M}^T$ . And then, we define the one-step-rollback estimation on  $p$ -th parameter in the  $\hat{\Theta}$  as  $\hat{\Theta}_p^{(j)}$ , that is, replace the  $p$ -th parameter in MLE by its estimate in  $j$ -th iteration. For example, if  $\hat{a}_1$  is the  $p$ -th element in  $\hat{\Theta}$ ,  $\hat{\Theta}_p^{(j)}$  can be written as  $(\hat{\epsilon}_1^{(0)}, \hat{\epsilon}_1^{(1)}, a_1^{(j)}, \hat{b}_1, \dots, \hat{\epsilon}_M^{(0)}, \hat{\epsilon}_M^{(1)}, \hat{a}_M, \hat{b}_M)^T$ .

---

**Algorithm 3** The SEM algorithm for Variance-covariance Matrix

---

**Input:** The MLE of parameters,  $\hat{\Theta}$ , and the estimated parameters in  $j$ -th iteration,  $\Theta^{(j)}$ .  
**for**  $p = 1$  to  $|\hat{\Theta}|$  **do**

Write  $\hat{\Theta}_p^{(j)}$ , the one-step-rollback estimation on the  $p$ -th parameter in the  $\hat{\Theta}$ .

Treat  $\hat{\Theta}_p^{(j)}$  as current estimation, and run one iteration of EM to obtain  $\tilde{\Theta}_p^{(j+1)}$ .

The  $p$ -th row of  $\frac{\partial \mathcal{F}}{\partial \Theta}$  can be calculated as  $\frac{\tilde{\Theta}_p^{(j+1)} - \hat{\Theta}}{\Theta^{(j)}(p) - \hat{\Theta}(p)}$ , where  $\hat{\Theta}(p)$  stands for the  $p$ -th element in  $\hat{\Theta}$  and similar for  $\Theta^{(j)}$ .

**end for**

Repeat this algorithm on all iteration  $j$ , until values in  $\frac{\partial \mathcal{F}}{\partial \Theta}$  become stable.

**Output:**  $\frac{\partial \mathcal{F}}{\partial \Theta}$ .

---

As the second key part in (24),  $\mathbf{I}_{oc}^{-1}$  is the inverse of the observed data information matrix evaluated at MLE. Similar to the situation discussed in Meng and Rubin (1991), the direct computation of the observed data information matrix is very difficult. We thus first calculate the complete data information matrix  $\mathbf{I}_c$  and then take its expectation over the conditional distribution  $f(\mathbf{S}, \mathbf{Z} \mid \mathbf{X}, \Theta)$  evaluated at  $\Theta = \hat{\Theta}$ . The complete data information matrix  $\mathbf{I}_c$  is calculated by  $\mathbf{I}_c(\Theta \mid \mathbf{X}, \mathbf{S}, \mathbf{Z}) = -\frac{\partial^2 \log f(\mathbf{X}, \mathbf{S}, \mathbf{Z} \mid \Theta)}{\partial \Theta^2}$ , which fully depends on the complete data likelihood. We have that  $\mathbf{I}_{oc} = E[\mathbf{I}_c(\Theta \mid \mathbf{X}, \mathbf{S}, \mathbf{Z}) \mid \mathbf{X}, \Theta]_{\Theta = \hat{\Theta}}$ . That is,  $\Theta = (\epsilon_1^{(0)}, \epsilon_1^{(1)}, a_1, b_1, \dots, \epsilon_M^{(0)}, \epsilon_M^{(1)}, a_M, b_M)$ , and  $\mathbf{I}_{oc}$  is in a format of sparse block diagonal

matrix,

$$\begin{Bmatrix} \mathbf{I}_{oc}^{(1)} & 0 & 0 & 0 \\ 0 & \mathbf{I}_{oc}^{(2)} & 0 & 0 \\ 0 & 0 & \cdots & 0 \\ 0 & 0 & 0 & \mathbf{I}_{oc}^{(M)} \end{Bmatrix}$$

Combining the above two parts could give the estimate of the variance-covariance matrix,

V. Our limited numerical experiment suggests that this method works properly.

## B Additional Results in Data Analysis

### B.1 Results from 3-Cluster Model

$$\hat{\mathbf{\Pi}}_1 = \begin{bmatrix} 0.848 & 0.127 & 0.025 \\ 0.060 & 0.794 & 0.146 \\ 0.017 & 0.186 & 0.796 \end{bmatrix}, \hat{\mathbf{\Pi}}_2 = \begin{bmatrix} 0.795 & 0.205 & 0.000 \\ 0.000 & 0.994 & 0.006 \\ 0.000 & 0.001 & 0.999 \end{bmatrix}, \hat{\mathbf{\Pi}}_3 = \begin{bmatrix} 0.938 & 0.057 & 0.005 \\ 0.013 & 0.924 & 0.063 \\ 0.001 & 0.067 & 0.932 \end{bmatrix}.$$

$$\hat{\boldsymbol{\pi}}_1 = \begin{bmatrix} 0.213 & 0.443 & 0.344 \end{bmatrix}, \hat{\boldsymbol{\pi}}_2 = \begin{bmatrix} 0.000 & 0.089 & 0.911 \end{bmatrix}, \hat{\boldsymbol{\pi}}_3 = \begin{bmatrix} 0.106 & 0.459 & 0.435 \end{bmatrix}.$$

The numbers of QDs in the three clusters are as follows.

Cluster	1	2	3
Count	28	54	46

### B.2 Results from 4-Cluster Model

$$\hat{\mathbf{\Pi}}_1 = \begin{bmatrix} 0.842 & 0.133 & 0.025 \\ 0.067 & 0.784 & 0.149 \\ 0.022 & 0.212 & 0.766 \end{bmatrix}, \hat{\mathbf{\Pi}}_2 = \begin{bmatrix} 0.799 & 0.201 & 0.000 \\ 0.000 & 0.993 & 0.007 \\ 0.000 & 0.001 & 0.999 \end{bmatrix},$$

$$\hat{\mathbf{\Pi}}_3 = \begin{bmatrix} 0.899 & 0.085 & 0.016 \\ 0.017 & 0.842 & 0.141 \\ 0.002 & 0.082 & 0.917 \end{bmatrix}, \hat{\mathbf{\Pi}}_4 = \begin{bmatrix} 0.946 & 0.053 & 0.001 \\ 0.014 & 0.941 & 0.045 \\ 0.001 & 0.094 & 0.905 \end{bmatrix}.$$



$$\hat{\boldsymbol{\pi}}_1 = \begin{bmatrix} 0.234 & 0.453 & 0.313 \end{bmatrix}, \quad \hat{\boldsymbol{\pi}}_2 = \begin{bmatrix} 0.000 & 0.091 & 0.909 \end{bmatrix},$$

$$\hat{\boldsymbol{\pi}}_3 = \begin{bmatrix} 0.066 & 0.342 & 0.592 \end{bmatrix}, \quad \hat{\boldsymbol{\pi}}_4 = \begin{bmatrix} 0.155 & 0.574 & 0.271 \end{bmatrix}.$$

The numbers of QDs in the four clusters are as follows.

Cluster	1	2	3	4
Count	23	53	27	25

From the 3-cluster model to the 4-cluster model, the correspondence of the cluster assignments are as follows.

	1	2	3
1	23	0	0
2	0	53	0
3	5	1	21
4	0	0	25

In the 4-cluster model, Clusters 1 and 2 align well with Clusters 1 and 2 in the 3-cluster model. The estimated transition matrices and the equilibrium distributions for these two clusters closely match those from the 3-cluster model. It is clear that Clusters 3 and 4 in the 4-cluster model are mainly from splitting Cluster 3 in the 3-cluster model. Specifically, the new Cluster 3 is associated with a greater proportion of time spent in the high state, while the new Cluster 4 exhibits longer durations in the medium state. From the perspective of the transition matrices, the new Cluster 3 demonstrates a higher probability of transitioning to and remaining in the high state, as evidenced by the last column of  $\hat{\boldsymbol{\Pi}}_3$ . Conversely, the new Cluster 4 is characterized by a stronger tendency to remain in the medium state compared to the new Cluster 3.

### B.3 Results from 5-Cluster Model

$$\hat{\Pi}_1 = \begin{bmatrix} 0.814 & 0.16 & 0.026 \\ 0.073 & 0.774 & 0.153 \\ 0.029 & 0.28 & 0.692 \end{bmatrix}, \quad \hat{\Pi}_2 = \begin{bmatrix} 0.000 & 1.000 & 0.000 \\ 0.000 & 0.993 & 0.007 \\ 0.000 & 0.000 & 1.000 \end{bmatrix}, \quad \hat{\Pi}_3 = \begin{bmatrix} 0.889 & 0.092 & 0.019 \\ 0.036 & 0.785 & 0.179 \\ 0.006 & 0.132 & 0.863 \end{bmatrix},$$

$$\hat{\Pi}_4 = \begin{bmatrix} 0.936 & 0.063 & 0.001 \\ 0.024 & 0.922 & 0.055 \\ 0.002 & 0.154 & 0.844 \end{bmatrix}, \quad \hat{\Pi}_5 = \begin{bmatrix} 0.929 & 0.051 & 0.021 \\ 0.003 & 0.944 & 0.053 \\ 0.001 & 0.041 & 0.958 \end{bmatrix}.$$

$$\hat{\pi}_1 = \begin{bmatrix} 0.236 & 0.497 & 0.267 \end{bmatrix}, \quad \hat{\pi}_2 = \begin{bmatrix} 0.000 & 0.049 & 0.951 \end{bmatrix}, \quad \hat{\pi}_3 = \begin{bmatrix} 0.144 & 0.363 & 0.493 \end{bmatrix},$$

$$\hat{\pi}_4 = \begin{bmatrix} 0.219 & 0.577 & 0.203 \end{bmatrix}, \quad \hat{\pi}_5 = \begin{bmatrix} 0.025 & 0.427 & 0.548 \end{bmatrix}.$$

The numbers of QDs in the five clusters are as follows.

	1	2	3	4	5
Count	13	51	23	18	23

From the 4-cluster model to the 5-cluster model, the correspondence of the cluster assignments are as follows.

	1	2	3	4
1	13	0	0	0
2	0	51	0	0
3	8	0	15	0
4	2	0	0	16
5	0	2	12	9

Again, it can be seen that Clusters 1 and 2 maintain stability in their composition as the number of clusters increases, whereas the rest of the QDs undergoes progressive subdivisions driven by differences in time spent in medium and high states. Using the 3-cluster model as a reference, the newly formed clusters in the 5-cluster model (Clusters 3–5) predominantly

emerge from subdivisions within Cluster 3, with minimal contributions from Clusters 1 and 2.